

---

# DF<sup>2</sup>: Distribution-Free Decision-Focused Learning

---

Lingkai Kong, Wenhao Mu, Jiaming Cui Yuchen Zhuang  
 B. Aditya Prakash Bo Dai Chao Zhang

College of Computing  
 Georgia Institute of Technology

{lkkong, wmu30, jiamingcui1997, yczhuang, badityap, bodai, chaozhang}@gatech.edu

## Abstract

Decision-focused learning (DFL) has recently emerged as a powerful approach for predict-then-optimize problems by customizing a predictive model to a downstream optimization task. However, existing end-to-end DFL methods are hindered by three significant bottlenecks: model mismatch error, sample average approximation error, and gradient approximation error. Model mismatch error stems from the misalignment between the model’s parameterized predictive distribution and the true probability distribution. Sample average approximation error arises when using finite samples to approximate the expected optimization objective. Gradient approximation error occurs as DFL relies on the KKT condition for exact gradient computation, while most methods approximate the gradient for backpropagation in non-convex objectives. In this paper, we present DF<sup>2</sup> —the first *distribution-free* decision-focused learning method explicitly designed to address these three bottlenecks. Rather than depending on a task-specific forecaster that requires precise model assumptions, our method directly learns the expected optimization function during training. To efficiently learn the function in a data-driven manner, we devise an attention-based model architecture inspired by the distribution-based parameterization of the expected objective. Our method is, to the best of our knowledge, the first to address all three bottlenecks within a single model. We evaluate DF<sup>2</sup> on a synthetic problem, a wind power bidding problem, and a non-convex vaccine distribution problem, demonstrating the effectiveness of DF<sup>2</sup>.

## 1 Introduction

Many decision-making processes can be formulated as solving a stochastic optimization problem:

$$\arg \min_{\mathbf{a} \in C} \mathbb{E}_{\mathbf{y}} [f(\mathbf{y}, \mathbf{a})],$$

where  $\mathbf{y}$  represents the parameters of the optimization problem,  $\mathbf{a}$  denotes the decision variables within a feasible space  $C$ , and  $f$  is the cost function to be optimized. In many real-world applications, the parameters  $\mathbf{y}$  are *unknown* and *context-dependent*, requiring inference from correlated features  $\mathbf{x}$ . As an example, consider personalized medicine, where  $\mathbf{y}$  might represent patient-specific responses to different treatments,  $\mathbf{a}$  could be the selected treatments for each patient, and  $f$  would measure the discrepancy between the actual patient responses and the treatment outcomes. The task is to determine the optimal  $\mathbf{a}$  to minimize the cost  $f$ . In this context, patient-specific responses  $\mathbf{y}$  are typically unknown and must be predicted using features  $\mathbf{x}$  such as patient demographics, medical history, and genetic information.

In this paper, we assume a dataset  $\mathcal{D} = \{\mathbf{x}_i, \mathbf{y}_i\}_{i=1}^N$  drawn from the joint distribution of the features and parameters of the optimization problem  $p(\mathbf{x}, \mathbf{y})$ . Our objective is to learn a decision-making model with parameter  $\theta$  that takes features  $\mathbf{x}$  as input and produces optimal decisions  $\mathbf{a}^*$  at  $\mathbf{x}$ . The

model should be trained to output optimal decisions that minimize the expected decision cost under the joint distribution of  $(\mathbf{x}, \mathbf{y})$ :

$$\arg \min_{\theta} \mathbb{E}_{p(\mathbf{x}, \mathbf{y})} [f(\mathbf{y}, \mathbf{a}^*(\mathbf{x}; \theta))]. \quad (1)$$

Given the increasing capacity to train potent deep learning predictors, a common strategy to solve this problem is the so-called two-stage pipeline. This pipeline involves learning a probabilistic predictive model for the unknown parameters in the prediction stage with a generic loss for model fitting (*e.g.*, negative log-likelihood), which will be used for stochastic optimization problem in the optimization stage. Despite its popularity, this two-stage approach relies on an assumption that better prediction in terms of the prediction loss always leads to better optimization outcomes—an assumption that often proves imprecise due to the non-uniform impact of prediction errors on the optimization loss. In contrast, Decision-focused Learning (DFL) [11, 1, 55, 46, 57] integrates prediction and optimization layers into a unified model by leveraging the implicit function theorem and KKT conditions to differentiate through the optimization problem. This approach tailors the prediction layer for the optimization task, leading to learning for decision-making through regret minimization.

Despite the promising results of DFL, there are several significant bottlenecks in current DFL methods due to the nature of optimization and prediction integration: (1) Model mismatch error: real-world applications often operate in highly uncertain environments and involve complex, multimodal probability distributions. In contrast, DFL requires simple parametrized distribution models for computational feasibility, leading to a mismatch. (2) Sample average approximation error: When there is no closed-form expression for the expected optimization objective, we typically draw a finite number of samples from the distribution for averaging, which will introduce extra statistical errors. (3) Gradient approximation error: DFL relies on the KKT conditions for differentiating through the optimization solver. However, the KKT condition is only a necessary condition for optimal solution of convex problem, which is unable to characterize the optimal solution in non-convex setting, and thus, will lead to inaccuracies that cumulatively result in lower decision quality. The recent SO-EBM model [27] proposes a surrogate objective to bypass the gradient computation challenges. However, it is still model-based and suffers from the other two bottlenecks. To the best of our knowledge, there is no existing DFL method that can address all three bottlenecks within a single model.

We propose DF<sup>2</sup>—the first distribution-free decision-focused learning method, to explicitly address the three bottlenecks. Instead of relying on a task-specific forecaster that necessitates precise model assumptions, we propose to learn directly the expectation of the optimization objective function from the data. Upon learning, we can obtain the optimal decision by maximizing the learned expected function within the feasible space. In order to ensure that the network architecture lies within the true model class and minimize bias error, we have developed an attention-based network architecture that emulates the distribution-based parameterization of the expected objective. This attention architecture also preserves the convexity of the original optimization objective. In contrast to the two-stage model, DF<sup>2</sup> is decision-aware; in comparison to DFL methods, DF<sup>2</sup> removes the need for sampling, solving, and differentiating through the stochastic optimization problem during training, thereby avoiding the three bottlenecks.

Our main contributions can be summarized as follows: (1) We propose a distribution-free training objective for DFL. It avoids the three bottlenecks of existing DFL methods. (2) We propose an attention-based network architecture inspired by the distribution-based parameterization to ensure the network architecture is within the true model class. (3) Experiments on synthetic data, wind power bidding and COVID-19 vaccine distribution show that our method can achieve better performance than existing DFL methods.

## 2 Bottlenecks of Decision-Focused Learning

DFL combines prediction and optimization into a single end-to-end model, thereby customizing the predictive model for the optimization task. By directly optimizing the task cost, the gradient of the model parameters can be calculated using the chain rule:  $\frac{df(\mathbf{y}, \mathbf{a}^*(\mathbf{x}; \theta))}{d\theta} = \frac{df(\mathbf{y}, \mathbf{a}^*(\mathbf{x}; \theta))}{d\mathbf{a}^*(\mathbf{x}; \theta)} \frac{d\mathbf{a}^*(\mathbf{x}; \theta)}{d\mathbf{y}} \frac{d\mathbf{y}}{d\theta}$ .

To compute the Jacobian  $\frac{d\mathbf{a}^*(\mathbf{x}; \theta)}{d\mathbf{y}}$  for backpropagation, OptNet [3] assumes quadratic optimization objectives and differentiates through the KKT conditions using the implicit function theorem. This way, OptNet can obtain the Jacobian by solving the optimization problem along with a set of linear equations in each training iteration. Later works [1, 46] extend this technique to general convex cost

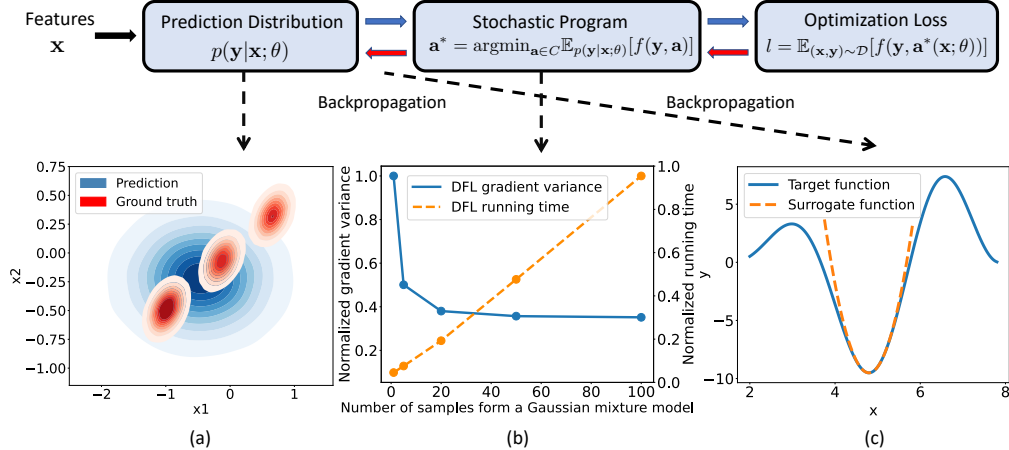


Figure 1: Decision-focused learning directly optimizes the task loss and leads to better decision regret. However, it suffers from three significant bottlenecks. More illustrations are in Section 2.

functions. Although DFL can achieve better decisions compared to two-stage learning, they have three significant bottlenecks which we will detail below.

**Bottleneck 1: Model Mismatch Error.** Real-world applications often involve complex and multi-modal probability distributions  $p(y|x)$ . One prominent example is the wind power forecasting task, where the environment exhibits high uncertainty due to the dynamic and stochastic nature of wind patterns. Factors such as changing weather conditions, terrain, and turbulence can significantly affect the true distribution of wind power, making it highly intricate and challenging to model accurately.

However, existing DFL approaches [11, 27] tend to assume simple distributions, *e.g.*, isotropic Gaussian distribution, for computational feasibility. However, this assumption can lead to considerable misalignment between the model’s parameterized distribution and the true underlying distribution in tasks with high uncertainty. This mismatch results in poor approximations and reduced decision-focused learning performance. Fig. 1(a) illustrates this issue using a ground-truth distribution composed of a mixture of three Gaussians. As we can see, the performances of DFL approaches suffer due to the model mismatch error, which is particularly pronounced in tasks with highly uncertain environments.

**Bottleneck 2: Sample Average Approximation Error.** In complex optimization problems, closed-form expressions for expectations might be unavailable, necessitating the use of sample average approximation [23, 51, 26]. Although adopting a more expressive distribution, such as a mixture density network, could potentially improve performance, doing so introduces another issue—sample approximation error. As shown in Fig. 1(b), when dealing with intricate distributions, increasing the sample size reduces the gradient variance slowly but demands substantially higher computational resources and longer running times.

**Bottleneck 3: Gradient Approximation Error.** Decision-focused learning relies on KKT condition to differentiate through the optimization problem. However, many real-world applications involve complicated non-convex objectives. Though [36, 54] propose to approximate the non-convex objectives by a quadratic function around a local minimum to approximate  $\frac{da^*}{dy}$  (Fig. 1(c)), the inaccurate gradients may be aggregated during the training iterations and thus lead to poor decision quality.

### 3 Additional Related Work

Several recent works have attempted to mitigate the gradient approximation error by avoiding differentiating through the optimization problem during training. However, they are all model-based and still suffer from the model mismatch error and sample average approximation error. SO-EBM [27] proposes a surrogate learning objective by maximizing the likelihood of the pre-computed optimal decision within an energy-based probability parameterization. LODL [41] approximates the decision-focused loss around the ground-truth parameter  $y$  with a quadratic function. Our method is different from it: (1) It assumes a deterministic setting while we assume the problem parameter  $y$  is a

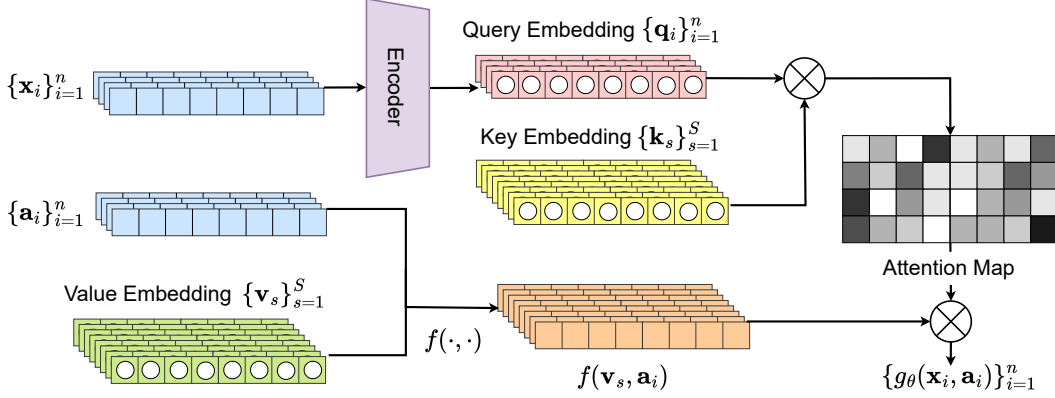


Figure 2: The proposed attention-based network architecture of  $DF^2$ . The network contains an encoder and a set of learnable attention points  $\{\mathbf{k}_s, \mathbf{v}_s\}_{s=1}^S$ . Given an input feature  $\mathbf{x}$ , the encoder first project it to query embedding space and then compute the attention weights by its dot product with the key embeddings. The final function value  $g(\mathbf{x}, \mathbf{a})$  is a weighted combination of  $f(\mathbf{v}, \mathbf{a})$ . The designed network architecture can effectively reduce the bias error in Proposition 1.

probability distribution. Therefore, this method is not directly applicable to our stochastic setting. (2) It approximates the decision loss while  $DF^2$  learns the expected cost function.

When the optimization problem is discrete, differentiating through the optimization layer is even more challenging since the gradient is ill-defined in the discrete domain. [56] relaxes the discrete decision into its continuous counterpart and adds a quadratic regularization term for linear objectives. [33] proposes a log barrier regularizer and differentiates through the homogeneous self-dual embedding. Our method is directly applicable to the discrete setting and we leave it for future exploration.

There are also approaches where a policy network is trained to directly map from the input to the solution of the optimization problem using supervised or reinforcement learning [52, 22, 28], in the learning to optimize community. Though these methods no longer suffer from these three bottlenecks, their performance are often inferior to DFL in the predict-then-optimize problem as they ignore the algorithmic structure of the problem and typically require a large amount of data to rediscover the algorithmic structure.

## 4 Distribution-Free Decision-Focused Learning

In this section, we introduce  $DF^2$  which explicitly addresses all the three bottlenecks within a single model. We first introduce the distribution-free training objective which transforms DFL into a function approximation problem. Then, we design an attention-based network architecture inspired by the distribution-based parameterization to reduce the bias error. Finally, we discuss how to obtain the optimal decision at inference time.

### 4.1 Distribution-Free Training Objective

Existing DFL methods primarily rely on a distribution-based approach. These techniques learn a forecaster that outputs probability distribution  $p(\mathbf{y}|\mathbf{x})$  based on various model assumptions. However, a more straightforward approach is to estimate the expected cost function  $\mathbb{E}_{p(\mathbf{y}|\mathbf{x})}[f(\mathbf{y}, \mathbf{a})]$  directly from the training data  $\mathcal{D} = \{\mathbf{x}_i, \mathbf{y}_i\}_{i=1}^N$ .

The cornerstone of our method is the observation that the expected cost objective is only a function of  $\mathbf{a}$  and  $\mathbf{x}$ , which is represented as  $g(\mathbf{x}, \mathbf{a}) = \mathbb{E}_{p(\mathbf{y}|\mathbf{x})}[f(\mathbf{y}, \mathbf{a})]$ . We propose a direct approach to learn a neural network with parameters  $\theta$  to match the expected cost function  $\mathbb{E}_{p(\mathbf{y}|\mathbf{x})}f(\mathbf{y}, \mathbf{a})$ . Our objective is to minimize the mean square error (MSE) between the fitted function  $g(\mathbf{x}, \mathbf{a})$  and the cost function  $f(\mathbf{y}, \mathbf{a})$  sampled from  $p(\mathbf{x}, \mathbf{y})$ :

$$g^*(\mathbf{x}, \mathbf{a}) = \arg \min_g \mathbb{E}_a \mathbb{E}_{(\mathbf{x}, \mathbf{y}) \sim \mathcal{D}} [g(\mathbf{x}, \mathbf{a}) - f(\mathbf{y}, \mathbf{a})]^2. \quad (2)$$

The proposed training objective can be efficiently optimized using stochastic gradient-based methods such as ADAM [24].

In the ideal case, when we have infinite training data and model capacity, the optimal solution  $g^*$  of Eq. 2 is the ground-truth conditional expectation  $\mathbb{E}_{p(\mathbf{y}|\mathbf{x})}[f(\mathbf{y}, \mathbf{a})]$ . Upon learning the optimal function, the optimal action can be derived by maximizing the fitted function  $\mathbf{a}^* = \arg \min_{\mathbf{a} \in C} g_\theta(\mathbf{x}, \mathbf{a})$ . However, in practical situations where training data and model capacity are limited, we obtain the expected error on the test set as the following proposition.

**Proposition 1.** *The expected MSE of the optimal solution  $g^*$  on the test set is:*

$$MSE_{\text{test}} = \underbrace{\mathbb{E}_{\mathcal{D}'} \left[ \left( g_{\mathcal{D}'}^*(\mathbf{x}, \mathbf{a}) - \mathbb{E}_{p(\mathbf{y}|\mathbf{x})}[f(\mathbf{y}, \mathbf{a})] \right)^2 \right]}_{\text{Bias}} + \underbrace{\mathbb{E}_{\mathcal{D}'} \left[ \left( g_{\mathcal{D}'}^*(\mathbf{x}, \mathbf{a}) - \mathbb{E}_{\mathcal{D}'}[g_{\mathcal{D}'}^*(\mathbf{x}, \mathbf{a})] \right)^2 \right]}_{\text{Variance}}, \quad (3)$$

where  $\mathcal{D}'$  denotes the training dataset augmented with the sampled actions  $\mathbf{a}$ .

*Proof.* See supplementary material for a detailed proof.

**Sampling Action from the Relaxed Constrained Space.** In practice, it's unnecessary to fit the true objective across the entire Euclidean space. Instead, we only need to sample from the constrained space  $C$ . However, even when the constrained space is convex, uniformly sampling from it can be non-trivial and may require time-consuming Markov chain Monte Carlo (MCMC) methods [15]. Hence, we propose to sample from a relaxed constrained space, such as a box. This allows us to sample each dimension of  $\mathbf{a}$  independently from a uniform distribution. Moreover, many predict-then-optimize problems are resource allocation problems where the decision variable  $\mathbf{a}$  is a simplex; for a simplex, we can directly sample from the Dirichlet distribution.

In contrast with DFL, our framework effectively transforms decision-focused learning into a function approximation problem, circumventing the complexities of solving and differentiating through the optimization problem. Thus, our framework avoids the three bottlenecks outlined in Section 2 that existing DFL methods encounter.

As we can see from Proposition 1, the test MSE consists of the bias and variance terms. The variance term will be reduced by sampling more data. To ensure that the bias error term approaches zero with more training data, it is crucial to keep the network architecture within the model class. To tackle this challenge, we introduce an attention-based network architecture in the following subsection.

## 4.2 Distribution-Based Parameterization

The key of our architecture design is to mimic the distribution-based parameterization of the expected cost function. Since our training objective bypass the need of sampling, solving and differentiating through the stochastic optimization problem, we can adopt an expressive non-parametric distribution with kernel conditional mean embedding (CME) to parameterize our model. The proposed network architecture can lead to zero bias error in Proposition 1

CME [44, 42] is a powerful tool to compute the expectation of a function in the reproducing kernel Hilbert space (RKHS), without the curse of dimensionality. Let  $\mathcal{F}$  be a RKHS over the domain of  $\mathbf{y}$  with kernel function  $\mathcal{R}_y(\mathbf{y}, \mathbf{y}')$  and inner product  $\langle \cdot, \cdot \rangle_{\mathcal{F}}$ . For a particular  $\mathbf{a}$ , we denote the corresponding function as  $f_a(\mathbf{y})$ . CME projects the conditional distribution to its expected feature map  $\mu_{\mathbf{y}|\mathbf{x}} \triangleq \mathbb{E}_{p(\mathbf{y}|\mathbf{x})}[\mathcal{R}_y(\mathbf{y}, \cdot)]$  and evaluates the conditional expectation of any RKHS function,  $f_a \in \mathcal{F}$ , as an inner product in  $\mathcal{F}$  using the reproducing property:

$$\mathbb{E}_{p(\mathbf{y}|\mathbf{x})}[f_a] = \int p(\mathbf{y}|\mathbf{x}) \langle \mathcal{R}_y(\mathbf{y}, \cdot), f_a \rangle_{\mathcal{F}} d\mathbf{y} = \left\langle \int p(\mathbf{y}|\mathbf{x}) \mathcal{R}_y(\mathbf{y}, \cdot) d\mathbf{y}, f_a \right\rangle_{\mathcal{F}} = \langle \mu_{\mathbf{y}|\mathbf{x}}, f_a \rangle_{\mathcal{F}}. \quad (4)$$

Assume that for all  $f_a \in \mathcal{F}$ , the conditional expectation  $\mathbb{E}_{p(\mathbf{y}|\mathbf{x})}[f_a(\mathbf{y})]$  is an element of the RKHS over the domain of  $\mathbf{x}$ , the conditional embedding can be estimated with a finite dataset  $\{\mathbf{x}_s, \mathbf{y}_s\}_{s=1}^S$  as  $\hat{\mu}_{\mathbf{y}|\mathbf{x}} = \sum_{s=1}^S \beta_s(\mathbf{x}) \mathcal{R}(\mathbf{y}_s, \cdot)$ , where  $\beta_s$  is a real-valued weight and can be computed with matrix calculation (see more details about this computation in the supplementary material).

One advantage of CME is that  $\hat{\mu}_{\mathbf{y}|\mathbf{x}}$  can converge to  $\mu_{\mathbf{y}|\mathbf{x}}$  in the RKHS norm at an overall rate of  $\mathcal{O}(S^{-\frac{1}{2}})$  [44], which is independent of the input dimensions. This property let CME works well in the high-dimensional space.

With the estimated CME, the conditional expectation can be computed by the reproducing property:

$$\mathbb{E}_{p(\mathbf{y}|\mathbf{x})}[f_{\mathbf{a}}(\mathbf{y})] = \langle \hat{\mu}_{\mathbf{y}|\mathbf{x}}, f_{\mathbf{a}} \rangle_{\mathcal{F}} = \left\langle \sum_{s=1}^S \beta_s(\mathbf{x}) \mathcal{R}_{\mathbf{y}}(\mathbf{y}_s, \cdot), f_{\mathbf{a}} \right\rangle_{\mathcal{F}} = \sum_{i=1}^N \beta_s(\mathbf{x}) f_{\mathbf{a}}(\mathbf{y}_s) \quad (5)$$

As shown in Eq. 5, the formulation is essentially a weighted combination of  $f_{\mathbf{a}}(\mathbf{y}_s)$ , where the weights are conditioned on the input features  $\mathbf{x}$ . This observation inspires us to leverage attention-based parameterization to represent the function  $g(\mathbf{x}, \mathbf{a})$ . The attention mechanism forms the foundation of the transformer architecture [49] and has been successfully utilized across various deep learning applications [21, 12]. Recent works [58, 48] have explored the connection between attention and kernel, setting the theoretical groundwork for our approach.

Inspired by this, we introduce a set of learnable attention points  $\{\mathbf{k}_s, \mathbf{v}_s\}_{s=1}^S$ , where  $\mathbf{k}$  is the key embedding and  $\mathbf{v}$  is the corresponding value embedding. For an input  $\mathbf{x}$ , the encoder first maps it to the query embedding space  $\mathbf{q}$  and compute the attention weights by its product with the key embeddings. We set the value function as  $f(\mathbf{v}_s, \mathbf{a})$  and, consequently, reformulate the function  $g(\mathbf{x}, \mathbf{a})$  using the softmax attention mechanism [49]:

$$g(\mathbf{x}, \mathbf{a}) = \text{Softmax} \left( \left[ \frac{\mathbf{q}(\mathbf{x})^\top \mathbf{k}_1}{\sqrt{d}}, \dots, \frac{\mathbf{q}(\mathbf{x})^\top \mathbf{k}_S}{\sqrt{d}} \right] \right)^\top [f(\mathbf{v}_1, \mathbf{a}), \dots, f(\mathbf{v}_S, \mathbf{a})], \quad (6)$$

where  $d$  is the dimension size of the key and value embeddings.

**Proposition 2.** *It holds for any  $\mathbf{x}$  and  $\mathbf{a}$ , the function  $g(\mathbf{x}, \mathbf{a})$  defined by the softmax attention in Eq. 6 satisfies  $g(\mathbf{x}, \mathbf{a}) = \mathbb{E}_{\hat{p}_{\mathcal{R}}(\mathbf{y}|\mathbf{x})}[f(\mathbf{y}, \mathbf{a})]$ , where  $\hat{p}_{\mathcal{R}}(\mathbf{y}|\mathbf{x})$  is a conditional kernel density estimator of  $p(\mathbf{y}|\mathbf{x})$ . Meanwhile, under the condition that  $\hat{p}_{\mathcal{R}}(\mathbf{y}|\mathbf{x}) \rightarrow p(\mathbf{y}|\mathbf{x})$  uniformly for any  $\mathbf{x}$  as  $S \rightarrow \infty$ , it holds that for  $S \rightarrow \infty$  that*

$$g(\mathbf{x}, \mathbf{a}) \rightarrow \mathbb{E}_{p(\mathbf{y}|\mathbf{x})}[f(\mathbf{y}, \mathbf{a})].$$

*Proof.* See supplementary material for a detailed proof.

The uniform convergence  $\hat{p}_{\mathcal{R}}(\mathbf{y}|\mathbf{x}) \rightarrow p(\mathbf{y}|\mathbf{x})$  holds when the density of  $p(\mathbf{x})$  is bounded from below [14]. As shown in Proposition 2, when the number of attention points goes to infinity, the bias error in Proposition 1 will go to zero. To speed up the training procedure, one can initialize the value embeddings of the attention points with randomly selected labels from the training dataset. This approach provides a reasonable starting point for the model and reduces the time it takes for the model to converge to a solution.

**Remark.** Our proposed attention-based network architecture represents a parameterization of  $p(\mathbf{y}|\mathbf{x})$ , drawing similarities with the two-stage model and DFL. Compared with the two-stage model, we learn the expected cost function to make DF<sup>2</sup> decision-aware. Compared with DFL, we do not have to solve the stochastic optimization problem during learning. As a result, we can adopt an expressive nonparametric distribution with CME to parameterize  $p(\mathbf{y}|\mathbf{x})$  and meanwhile bypass the three bottlenecks discussed in Section 2.

### 4.3 Model Inference

At test time, we can obtain the optimal decision by maximizing the learned expected cost function  $\arg \min_{\mathbf{a} \in \mathcal{C}} g(\mathbf{x}, \mathbf{a})$ . The final representation of  $g(\mathbf{x}, \mathbf{a})$  is a weighted combination of  $f(\mathbf{v}_s, \mathbf{a})$  with different value embeddings. Another benefit of the proposed attention-based network architecture is that it can preserve the convex property of the cost function.

**Proposition 3.** *As long as  $f(\mathbf{y}, \mathbf{a})$  is a convex function with respect to  $\mathbf{a}$ ,  $g(\mathbf{x}, \mathbf{a})$  is a convex function with respect to  $\mathbf{a}$ .*

*Proof:* This is a direct consequence of the theorem that a convex combination of convex functions remains a convex function

When the original objective is convex, we can use any existing black-box convex solver [10, 2]. For non-convex problem, we can use projected gradient descent.

It's worth noting that existing DFL methods also suffer from sample approximation error during the testing phase. Our method, however, eliminates this error as we directly learn the expected cost function  $g(\mathbf{x}, \mathbf{a})$  and hence, do not need to conduct sampling at inference time.

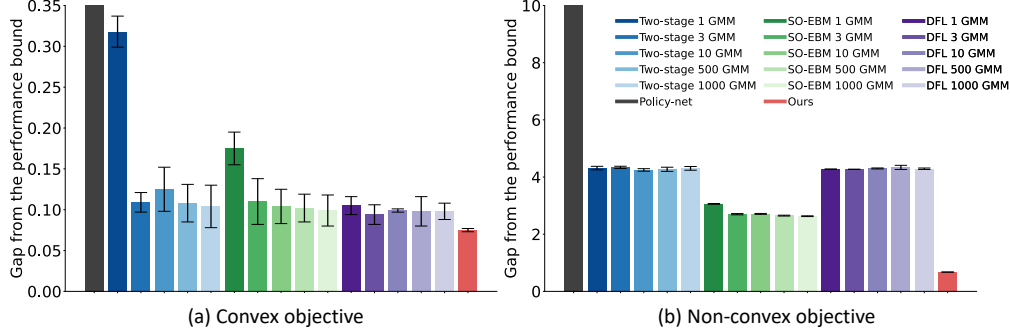


Figure 3: The gap of the model’s decision regret from the lower bound of the decision regret on the synthetic data for both the convex and non-convex objectives.

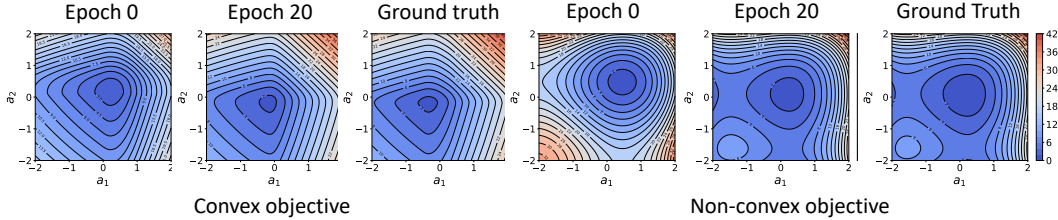


Figure 4: Randomly initialized landscape,  $DF^2$  recovered landscape and the ground-truth landscape on the synthetic data. The landscape is conditioned on an input feature sampled from the test set.

## 5 Experiments

In this section, we empirically evaluate  $DF^2$  and conduct experiments in three tasks: (1) A synthetic setting with both convex and non-convex objectives; (2) Wind power bidding with a convex objective; (3) Vaccine distribution for Covid-19 with a non-convex objective. Finally, we perform ablation studies to show the effect of each model design in  $DF^2$ .

### 5.1 Synthetic Data

To highlight the ability to learn the true expected objective, we first validate our method on a synthetic dataset where the true underlying model is known to us. To simulate the multi-modal scenario in the real world, we generate 5000 feature-parameter pairs using a Gaussian mixture model (GMM) with three components. We consider both convex and non-convex objectives. The details of the data generation process and the objective functions are provided in the supplementary material.

**Experimental Setup.** Since we know the true underlying data generation process for this synthetic setting, we compute the lower bound of the decision regret and use the gap of the model’s decision regret from this lower bound as the evaluation metric. We compare with the following baselines: (1) A two-stage model trained with negative log-likelihood. (2) Decision-focused learning (DFL). For the convex objective, we implement DFL using the `cvxpylayers` library [1] since it can accurately differentiate through convex objectives. For the non-convex objective, we first use a black-box solver to obtain the optimal solution and then approximate the original objective using a quadratic function around the optimal solution and thus it can fit into the `QPTH` library [3]. (3) SO-EBM [27]: It uses the energy-based model as a surrogate objective to speed up DFL. (4) Policy-net: It directly maps from the input features to the decision variables by minimizing the task loss using supervised learning.

For the two-stage model, DFL and SO-EBM, the forecasters use GMM with a different number of components and use 100 samples to estimate the expectation of the objective as we found that more samples bring little performance gain. For a fair comparison, we use the same backbone for the encoder of  $DF^2$  and the forecaster of the baselines and 1000 attention points for both the convex and non-convex objectives. Our supplementary provides more details of the experimental setup and model parameters.

**Results.** Fig. 3(a) shows the results on the convex objective for all the methods. As we can see,  $DF^2$  can outperform all the baselines. Even when the model assumption is aligned with the

ground truth distribution (3 GMM), DFL still underperforms  $DF^2$  since it suffers from the sample average approximation error. When we increase the model complexity beyond the ground truth, the performance of DFL even drops as the sample approximation error becomes more severe. The performance of SO-EBM is inferior to DFL because DFL can accurately differentiate through this convex objective while the training of SO-EBM requires importance sampling for the EBM and introduces additional approximation error. For the non-convex objective, the improvement of  $DF^2$  against the baselines becomes more significant as shown in Fig. 3(b). Specifically,  $DF^2$  reduces the gap from the performance bound by 74.3% compared with the strongest baseline SO-EBM. In this scenario, the performance of DFL is almost at the same level as the two-stage model. This is because the three bottlenecks of DFL aggregate with each other for this complicated objective and result in very poor decision-making performance.

Fig. 4 visualizes the learned expected function and the ground truth expectation on a test sample for both the convex and non-convex objectives. We found that the  $DF^2$  can effectively recover the landscape of the true expected cost function.

## 5.2 Wind Power Bidding

We next move on to a real-world wind power bidding problem with a convex objective. In this task, a wind power firm engages in both energy and reserve markets, given the generated wind power  $\mathbf{x} \in \mathbb{R}^{24}$  in the last 24 hours. The firm needs to decide the energy quantity  $\mathbf{a}_E \in \mathbb{R}^{12}$  to bid and quantity  $\mathbf{a}_R \in \mathbb{R}^{12}$  to reserve over the next 12-24 hours in advance, based on the forecasted wind power  $\mathbf{y} \in \mathbb{R}^{12}$ . The optimization objective is a piecewise function consisting of three segments [38, 5], which is to maximize the revenue of the energy sales while minimizing the penalties for decision inaccuracies of overbidding and underbidding [38, 5]. We provide more details of the optimization objective in the supplementary material.

**Experimental Setup.** We use the wind power generation dataset of a German energy company during 08/23/2019 to 09/22/2020 [40]. The forecaster of the two-stage model, DFL and SO-EBM is a two-layer long short-term memory networks (LSTM) [16] which takes the historical wind power in the last 24 hours as input features and outputs the forecasted wind power for the subsequent 12 to 24 hours. For a fair comparison,  $DF^2$  uses the same LSTM architecture as the encoder and 500 attention points. During training, the two-stage model, DFL and SO-EBM use 100 samples to estimate the expected objective as more samples provide little performance gain.

**Results.** Though this is a convex objective, our method can consistently outperform all the baselines by a significant margin even when the number of GMM components of baselines is larger than the attention points of  $DF^2$ . Specifically,  $DF^2$  can improve the decision regret by 5.8% compared with the strongest baseline. The wind power forecasting task is marked by high uncertainty, which makes it challenging to construct an accurate model assumption. Therefore, in this context, a more effective approach is to learn the expected cost function directly from the data, without imposing any parametric distribution assumption.

During the COVID-19 pandemic, computing a vaccine distribution strategy is one of the most challenging problems for epidemiologists and policymakers. In practice, meta-population Ordinary Differential Equations (ODEs) based epidemiological models [29, 34, 47] are widely used to predict and evaluate the outcomes of different vaccine distribution strategies, ultimately informing policy decisions [7, 13, 37]. These models rely on people mobility data, such as Origin-Destination (OD) matrices, to capture the pandemic spread dynamics across diverse locations [29, 20, 8, 37]. In this task, given the OD matrices  $\mathbf{x} \in \mathbb{R}^{47 \times 47 \times 7}$  of last week, *i.e.*,  $\mathbf{x}[i, j, t]$  represents the number of people move from region  $i$  to  $j$  on day  $t$ , we need to decide the vaccine distribution  $\mathbf{a} \in \mathbb{R}^{47}$  across the 47 regions in Japan with a budget constraint ( $\mathbf{a}[i]$  is the number of vaccines distributed to the

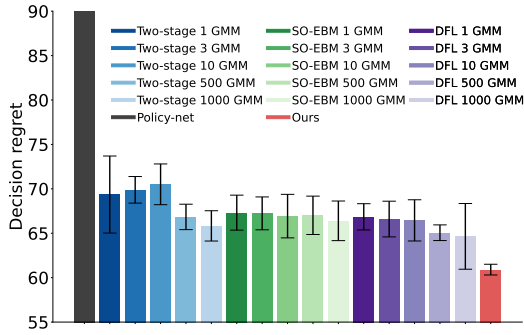


Figure 5: Decision regret on wind power bidding.



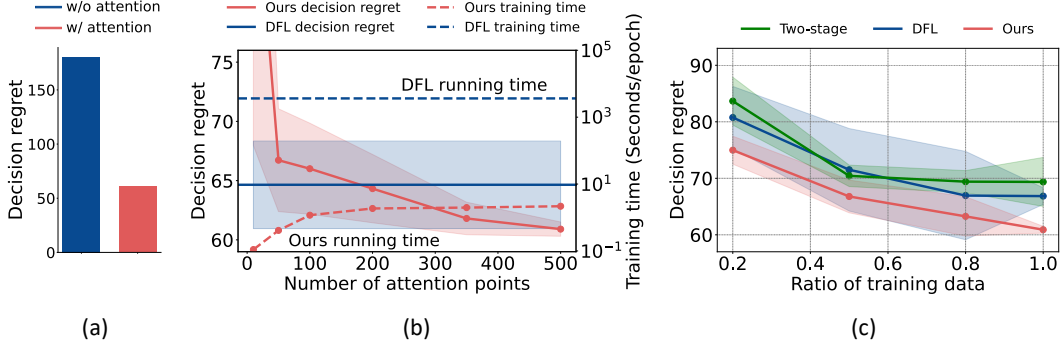


Figure 7: Ablation study on the wind power bidding problem.

region  $i$ ). The optimization objective is to minimize the total number of infected people over the ODE-driven dynamics, based on the forecasted OD matrices  $\mathbf{y} \in \mathbb{R}^{47 \times 47 \times 7}$  for the next week. This task is a challenging non-convex optimization problem due to the nonlinear ODE-based simulation model.

**Experimental Setup.** We use the OD matrices dataset of Japan [19] during 04/01/2020 to 02/28/2021. The two-stage model, DFL and SO-EBM use DC-RNN [31] as the forecaster which adopts an encoder-decoder architecture. The forecaster takes the OD matrices of last week as input features and predicts the OD matrices of next week. For a fair comparison,  $DF^2$  employs the same encoder in the network architecture and uses 100 attention points. During training, the two-stage model, DFL and SO-EBM use 100 samples to estimate the expected objective as more samples provide little performance gain.

**Results.** Fig. 6 shows the decision regret on the COVID-19 vaccine distribution problem for all the methods.  $DF^2$  can outperform the strongest baseline by 3.0% in terms of the decision regret. As we can see, on this challenging task, increasing the number of components in GMM cannot effectively improve the performance of DFL as it may suffer from a more severe sample approximation error.

### 5.3 Ablation Study

We investigate the effectiveness of each model design of  $DF^2$  via ablation studies on the wind power bidding problem. Fig. 7 shows the results and our findings can be summarized as follows: (1) Without the attention-based network architecture, we see a significant performance drop in Fig. 7(a). This is because, without the attention architecture, the network architecture may not be within the true model class and thus suffer from high bias error in Proposition 1. (2) Our model performance can be improved with more attention points as in Fig. 7(b). We also plot the decision regret and training time of DFL. We find that when the number of attention points is over 200,  $DF^2$  can outperform DFL in terms of the decision regret while being orders of magnitude faster. (3) Our method outperforms baselines constantly with different ratios of training data as shown in Fig. 7(c). The superior performance is because we use attention-based network architecture to mimic the distribution-based parameterization. Compared with the two-stage model, we are decision-aware; compared with DFL methods, we do not suffer from the three bottlenecks.

## 6 Limitations and Conclusion

We focus on addressing the three bottlenecks of existing decision-focused learning: (1) model mismatch error, (2) sample average approximation error, and (3) gradient approximation error. To this end, we propose  $DF^2$ —the first distribution-free DFL method which does not require any model assumption.  $DF^2$  adopts a distribution-free training objective that directly learns the expected cost

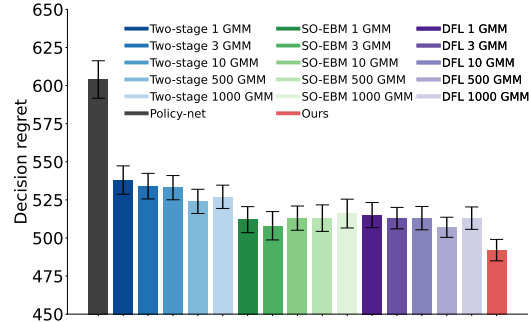


Figure 6: Decision regret on vaccine distribution.

function from the data. To reduce the bias error, we design an attention-based network architecture, drawing inspiration from the distribution-based parameterization of the expected cost function. Empirically, we demonstrate that  $DF^2$  is effective in a wide range of stochastic optimization problems with either convex or non-convex objectives.

Despite the strengths,  $DF^2$  does have limitations. Our approach primarily targets highly uncertain environments wherein  $p(\mathbf{y}|\mathbf{x})$  manifests as a complex multi-modal distribution. However, as detailed in the supplementary material, we conducted additional experiments with a convex inventory optimization problem based on forecasted store item demand. We find that DFL is slightly better than  $DF^2$ . Our analysis shows that it is because the store customer demand follows a simple distribution with low uncertainty. In this scenario, the model mismatch error and sample average approximation error of DFL are minimal. Moreover, DFL does not suffer from the gradient approximation error for the convex objective. Therefore, when the forecasting task exhibits low uncertainty and the optimization objective is convex, DFL is still a better method.

## References

- [1] Akshay Agrawal, Brandon Amos, Shane Barratt, Stephen Boyd, Steven Diamond, and J Zico Kolter. Differentiable convex optimization layers. *Advances in neural information processing systems*, 32, 2019.
- [2] Akshay Agrawal, Robin Verschueren, Steven Diamond, and Stephen Boyd. A rewriting system for convex optimization problems. *Journal of Control and Decision*, 5(1):42–60, 2018.
- [3] Brandon Amos and J Zico Kolter. Optnet: Differentiable optimization as a layer in neural networks. In *International Conference on Machine Learning*, pages 136–145. PMLR, 2017.
- [4] Amir Beck and Marc Teboulle. Mirror descent and nonlinear projected subgradient methods for convex optimization. *Operations Research Letters*, 31(3):167–175, 2003.
- [5] Di Cao, Weihao Hu, Xiao Xu, Tomislav Dragicevic, Qi Huang, Zhou Liu, Zhe Chen, and Frede Blaabjerg. Bidding strategy for trading wind energy and purchasing reserve of wind power producer – a drl based approach. *International Journal of Electrical Power and Energy Systems*, 117:105648, 2020.
- [6] Di Cao, Weihao Hu, Xiao Xu, Tomislav Dragicevic, Qi Huang, Zhou Liu, Zhe Chen, and Frede Blaabjerg. Bidding strategy for trading wind energy and purchasing reserve of wind power producer – a drl based approach. *International Journal of Electrical Power and Energy Systems*, 117:105648, 2020.
- [7] Estee Y Cramer, Evan L Ray, Velma K Lopez, Johannes Bracher, Andrea Brennen, Alvaro J Castro Rivadeneira, Aaron Gerding, Tilmann Gneiting, Katie H House, Yuxin Huang, et al. Evaluation of individual and ensemble probabilistic forecasts of covid-19 mortality in the united states. *Proceedings of the National Academy of Sciences*, 119(15):e2113561119, 2022.
- [8] Jiaming Cui, Arash Haddadan, ASM Ahsan-Ul Haque, Bijaya Adhikari, Anil Vullikanti, and B Aditya Prakash. Information theoretic model selection for accurately estimating unreported covid-19 infections. *medRxiv*, pages 2021–09, 2021.
- [9] Bo Dai, Niao He, Hanjun Dai, and Le Song. Provable bayesian inference via particle mirror descent. In *Artificial Intelligence and Statistics*, pages 985–994. PMLR, 2016.
- [10] Steven Diamond and Stephen Boyd. CVXPY: A Python-embedded modeling language for convex optimization. *Journal of Machine Learning Research*, 17(83):1–5, 2016.
- [11] Priya Donti, Brandon Amos, and J Zico Kolter. Task-based end-to-end model learning in stochastic optimization. *Advances in neural information processing systems*, 30, 2017.
- [12] Alexey Dosovitskiy, Lucas Beyer, Alexander Kolesnikov, Dirk Weissenborn, Xiaohua Zhai, Thomas Unterthiner, Mostafa Dehghani, Matthias Minderer, Georg Heigold, Sylvain Gelly, Jakob Uszkoreit, and Neil Houlsby. An image is worth 16x16 words: Transformers for image recognition at scale. In *International Conference on Learning Representations*, 2021.

- [13] IHME COVID-19 forecasting team. Modeling covid-19 scenarios for the united states. *Nature medicine*, 2020.
- [14] Jan G. De Gooijer and Dawit Zerom. On Conditional Density Estimation. *Statistica Neerlandica*, 57(2):159–176, May 2003.
- [15] Hulda S Haraldsdóttir, Ben Cousins, Ines Thiele, Ronan MT Fleming, and Santosh Vempala. Chrr: coordinate hit-and-run with rounding for uniform sampling of constraint-based models. *Bioinformatics*, 33(11):1741–1743, 2017.
- [16] Sepp Hochreiter and Jürgen Schmidhuber. Long short-term memory. *Neural computation*, 9(8):1735–1780, 1997.
- [17] Sepp Hochreiter and Jürgen Schmidhuber. Long short-term memory. *Neural computation*, 9(8):1735–1780, 1997.
- [18] Eric Jang, Shixiang Gu, and Ben Poole. Categorical reparameterization with gumbel-softmax. In *International Conference on Learning Representations*, 2017.
- [19] Renhe Jiang, Zhaonan Wang, Zekun Cai, and Chuang Yang. Countrywide origin-destination matrix prediction and its application for covid-19. <https://github.com/deepkashiwa20/ODCRN/tree/main/data>.
- [20] Morgan P Kain, Marissa L Childs, Alexander D Becker, and Erin A Mordecai. Chopping the tail: How preventing superspreading can help to maintain covid-19 control. *Epidemics*, 34:100430, 2021.
- [21] Jacob Devlin Ming-Wei Chang Kenton and Lee Kristina Toutanova. Bert: Pre-training of deep bidirectional transformers for language understanding. In *Proceedings of NAACL-HLT*, pages 4171–4186, 2019.
- [22] Elias Khalil, Hanjun Dai, Yuyu Zhang, Bistra Dilikina, and Le Song. Learning combinatorial optimization algorithms over graphs. *Advances in neural information processing systems*, 30, 2017.
- [23] Sujin Kim, Raghu Pasupathy, and Shane G Henderson. A guide to sample average approximation. *Handbook of simulation optimization*, pages 207–243, 2015.
- [24] Diederik P Kingma and Jimmy Ba. Adam: A method for stochastic optimization. In *International Conference on Representation Learning*, 2015.
- [25] Diederik P Kingma and Jimmy Ba. Adam: A method for stochastic optimization. *International Conference on Representation Learning*, 2015.
- [26] Anton J Kleywegt, Alexander Shapiro, and Tito Homem-de Mello. The sample average approximation method for stochastic discrete optimization. *SIAM Journal on Optimization*, 12(2):479–502, 2002.
- [27] Lingkai Kong, Jiaming Cui, Yuchen Zhuang, Rui Feng, B Aditya Prakash, and Chao Zhang. End-to-end stochastic optimization with energy-based model. In *Advances in Neural Information Processing Systems*, 2022.
- [28] Ke Li and Jitendra Malik. Learning to optimize. *arXiv preprint arXiv:1606.01885*, 2016.
- [29] Ruiyun Li, Sen Pei, Bin Chen, Yimeng Song, Tao Zhang, Wan Yang, and Jeffrey Shaman. Substantial undocumented infection facilitates the rapid dissemination of novel coronavirus (sars-cov-2). *Science*, 368(6490):489–493, 2020.
- [30] Ruiyun Li, Sen Pei, Bin Chen, Yimeng Song, Tao Zhang, Wan Yang, and Jeffrey Shaman. Substantial undocumented infection facilitates the rapid dissemination of novel coronavirus (sars-cov-2). *Science*, 368(6490):489–493, 2020.
- [31] Yaguang Li, Rose Yu, Cyrus Shahabi, and Yan Liu. Diffusion convolutional recurrent neural network: Data-driven traffic forecasting. In *International Conference on Learning Representations*, 2018.

- [32] Yaguang Li, Rose Yu, Cyrus Shahabi, and Yan Liu. Diffusion convolutional recurrent neural network: Data-driven traffic forecasting. In *International Conference on Learning Representations*, 2018.
- [33] Jayanta Mandi and Tias Guns. Interior point solving for lp-based prediction+ optimisation. *Advances in Neural Information Processing Systems*, 33:7272–7282, 2020.
- [34] Sen Pei, Sasikiran Kandula, and Jeffrey Shaman. Differential effects of intervention timing on covid-19 spread in the united states. *Science advances*, 6(49):eabd6370, 2020.
- [35] Sen Pei, Sasikiran Kandula, and Jeffrey Shaman. Differential effects of intervention timing on covid-19 spread in the united states. *Science advances*, 6(49):eabd6370, 2020.
- [36] Andrew Perrault, Bryan Wilder, Eric Ewing, Aditya Mate, Bistra Dilkina, and Milind Tambe. End-to-end game-focused learning of adversary behavior in security games. In *Proceedings of the AAAI Conference on Artificial Intelligence*, volume 34, pages 1378–1386, 2020.
- [37] Alexander Rodríguez, Anika Tabassum, Jiaming Cui, Jiajia Xie, Javen Ho, Pulak Agarwal, Bijaya Adhikari, and B. Aditya Prakash. Deepcovid: An operational deep learning-driven framework for explainable real-time covid-19 forecasting. *Proceedings of the AAAI Conference on Artificial Intelligence*, 35(17):15393–15400, May 2021.
- [38] Manassakan Sanayha and Peerapon Vateekul. Model-based deep reinforcement learning for wind energy bidding. *International Journal of Electrical Power and Energy Systems*, 136:107625, 2022.
- [39] Manassakan Sanayha and Peerapon Vateekul. Model-based deep reinforcement learning for wind energy bidding. *International Journal of Electrical Power and Energy Systems*, 136:107625, 2022.
- [40] Jorge Sandoval. Wind power generation data. <https://www.kaggle.com/datasets/jorgesandoval/wind-power-generation?select=TransnetBW.csv>.
- [41] Sanket Shah, Bryan Wilder, Andrew Perrault, and Milind Tambe. Learning (local) surrogate loss functions for predict-then-optimize problems. *Advances in Neural Information Processing Systems*, 2022.
- [42] Le Song, Kenji Fukumizu, and Arthur Gretton. Kernel embeddings of conditional distributions: A unified kernel framework for nonparametric inference in graphical models. *IEEE Signal Processing Magazine*, 30(4):98–111, 2013.
- [43] Le Song, Kenji Fukumizu, and Arthur Gretton. Kernel embeddings of conditional distributions: A unified kernel framework for nonparametric inference in graphical models. *IEEE Signal Processing Magazine*, 30(4):98–111, 2013.
- [44] Le Song, Jonathan Huang, Alex Smola, and Kenji Fukumizu. Hilbert space embeddings of conditional distributions with applications to dynamical systems. In *Proceedings of the 26th Annual International Conference on Machine Learning*, pages 961–968, 2009.
- [45] Le Song, Jonathan Huang, Alex Smola, and Kenji Fukumizu. Hilbert space embeddings of conditional distributions with applications to dynamical systems. In *Proceedings of the 26th Annual International Conference on Machine Learning*, pages 961–968, 2009.
- [46] Haixiang Sun, Ye Shi, Jingya Wang, Hoang Duong Tuan, H. Vincent Poor, and Dacheng Tao. Alternating differentiation for optimization layers. In *The Eleventh International Conference on Learning Representations*, 2023.
- [47] Shaun Truelove, Claire P Smith, Michelle Qin, Luke C Mullany, Rebecca K Borchering, Justin Lessler, Katriona Shea, Emily Howerton, Lucie Contamin, John Levander, et al. Projected resurgence of covid-19 in the united states in july—december 2021 resulting from the increased transmissibility of the delta variant and faltering vaccination. *Elife*, 11:e73584, 2022.

- [48] Yao-Hung Hubert Tsai, Shaojie Bai, Makoto Yamada, Louis-Philippe Morency, and Ruslan Salakhutdinov. Transformer dissection: An unified understanding for transformer’s attention via the lens of kernel. In *Proceedings of the 2019 Conference on Empirical Methods in Natural Language Processing and the 9th International Joint Conference on Natural Language Processing (EMNLP-IJCNLP)*, pages 4344–4353, 2019.
- [49] Ashish Vaswani, Noam Shazeer, Niki Parmar, Jakob Uszkoreit, Llion Jones, Aidan N Gomez, Łukasz Kaiser, and Illia Polosukhin. Attention is all you need. *Advances in neural information processing systems*, 30, 2017.
- [50] Ashish Vaswani, Noam Shazeer, Niki Parmar, Jakob Uszkoreit, Llion Jones, Aidan N Gomez, Łukasz Kaiser, and Illia Polosukhin. Attention is all you need. *Advances in neural information processing systems*, 30, 2017.
- [51] Bram Verweij, Shabbir Ahmed, Anton J Kleywegt, George Nemhauser, and Alexander Shapiro. The sample average approximation method applied to stochastic routing problems: a computational study. *Computational optimization and applications*, 24(2):289–333, 2003.
- [52] Oriol Vinyals, Meire Fortunato, and Navdeep Jaitly. Pointer networks. *Advances in neural information processing systems*, 28, 2015.
- [53] Matt P Wand and M Chris Jones. *Kernel smoothing*. CRC press, 1994.
- [54] Kai Wang, Andrew Perrault, Aditya Mate, and Milind Tambe. Scalable game-focused learning of adversary models: Data-to-decisions in network security games. In *AAMAS*, pages 1449–1457, 2020.
- [55] Kai Wang, Bryan Wilder, Andrew Perrault, and Milind Tambe. Automatically learning compact quality-aware surrogates for optimization problems. *Advances in Neural Information Processing Systems*, 33:9586–9596, 2020.
- [56] Bryan Wilder, Bistra Dilkina, and Milind Tambe. Melding the data-decisions pipeline: Decision-focused learning for combinatorial optimization. In *Proceedings of the AAAI Conference on Artificial Intelligence*, volume 33, pages 1658–1665, 2019.
- [57] Kai Yan, Jie Yan, Chuan Luo, Liting Chen, Qingwei Lin, and Dongmei Zhang. A surrogate objective framework for prediction+ programming with soft constraints. *Advances in Neural Information Processing Systems*, 34:21520–21532, 2021.
- [58] Yufeng Zhang, Boyi Liu, Qi Cai, Lingxiao Wang, and Zhaoran Wang. An analysis of attention via the lens of exchangeability and latent variable models. *arXiv preprint arXiv:2212.14852*, 2022.
- [59] Yufeng Zhang, Boyi Liu, Qi Cai, Lingxiao Wang, and Zhaoran Wang. An analysis of attention via the lens of exchangeability and latent variable models. *arXiv preprint arXiv:2212.14852*, 2022.

## 7 Supplementary Material for DF<sup>2</sup>: Distribution-Free Decision-Focused Learning

### Contents

7.1	Additional Experiments on Inventory Optimization . . . . .	15
7.2	Additional Ablation Studies . . . . .	16
7.3	Additional Background on Conditional Mean Embedding . . . . .	16
7.4	Proof of Proposition 1 . . . . .	17
7.5	Proof of Proposition 2 . . . . .	18
7.6	Experimental Details . . . . .	20
7.6.1	Synthetic Data . . . . .	20
7.6.2	Wind Power Bidding . . . . .	21
7.6.3	COVID-19 Vaccine Distribution . . . . .	22
7.6.4	Inventory Optimization . . . . .	24

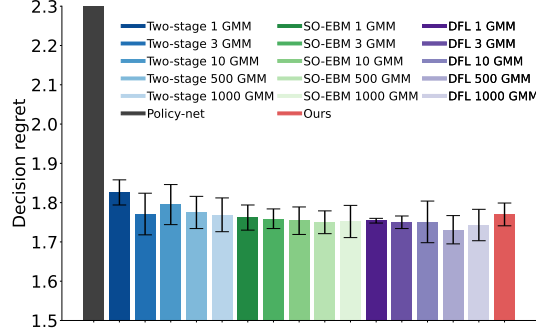


Figure 8: Decision regret on the inventory optimization task.

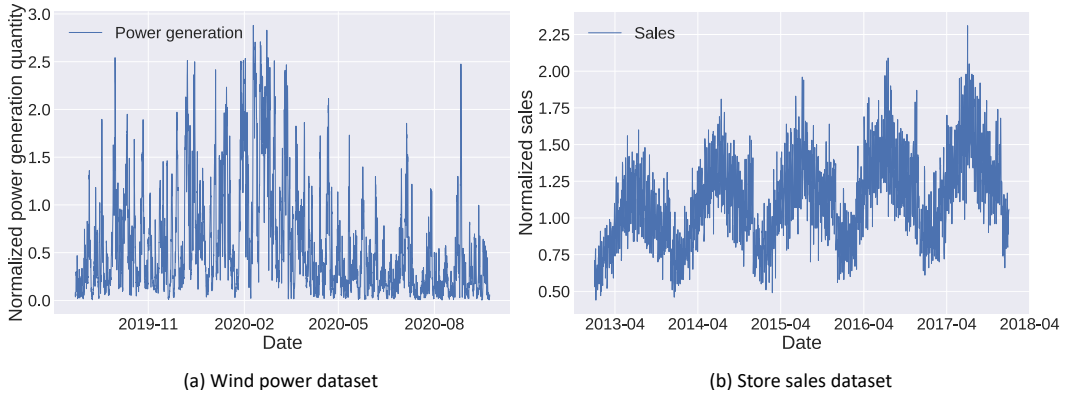


Figure 9: Visualization of the time-series data on the wind power and store sales datasets. The store sales dataset exhibits a strong periodicity with an overall rising trend, while the wind power dataset shows a more complex pattern with significant uncertainty.

## 7.1 Additional Experiments on Inventory Optimization

We also conducted experiments on a convex inventory optimization problem. In this task, a department store is tasked with predicting the sales  $\mathbf{y} \in \mathbb{R}^7$  for the upcoming 3rd-10th days based on the past 14 days’ sales data  $\mathbf{x} \in \mathbb{R}^{14}$  for a specific product, and accordingly, determining the best replenishment strategy  $\mathbf{a} \in \mathbb{R}^7$  for each day. The optimization objective is a combination of an under-purchasing penalty, an over-purchasing penalty, and a squared loss between supplies and demands:

$$\begin{aligned} & \text{minimize}_{\mathbf{a} \in \mathbb{R}^7} \mathbb{E}_{p(\mathbf{y}|\mathbf{x})} \sum_{i=1}^7 [20(\mathbf{y}[i] - \mathbf{a}[i])_+ + 5(\mathbf{a}[i] - \mathbf{y}[i])_+ + (\mathbf{a}[i] - \mathbf{y}[i])^2] \\ & \text{subject to } 0 \leq \mathbf{a}[i] \leq 3, \forall i, \end{aligned}$$

where  $(v)_+$  denote  $\max\{v, 0\}$ .

**Experiment Setup.** We use the store item demand dataset during 01/01/2013 to 12/31/2017<sup>1</sup>. The split ratio of the training dataset, validation dataset, and test dataset are 64%, 16%, 20%, respectively. The forecaster of the two-stage model, DFL and SO-EBM uses a two-layer long short-term memory network (LSTM) [17] as a feature extractor which is further stacked by a linear layer. The forecaster takes the historical item sales in the last 14 days as input features and outputs the forecasted item sales for the 3rd to 10th days in the future. The network has a hidden size of 128. For a fair comparison, DF<sup>2</sup> uses the same LSTM architecture as the encoder and 230 attention points. During training, the two-stage model, DFL and SO-EBM use 100 samples to estimate the expected objective as more samples provide little performance gain.

<sup>1</sup>The dataset is available at <https://www.kaggle.com/competitions/demand-forecasting-kernels-only/data?select=train.csv>

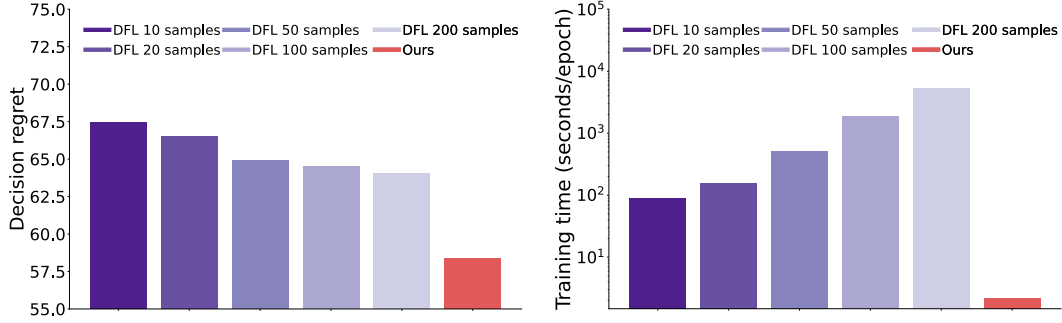


Figure 10: Additional ablation study 1 on the wind power bidding task.

**Results.** The decision regrets of all the methods are presented in Figure 8. From the results, we observe that DFL slightly outperforms  $DF^2$ . Additionally, we provide visualizations of the time-series data from the store sales dataset and the wind power dataset in Fig. 9. The store sales dataset exhibits a strong periodicity with an overall rising trend, while the wind power dataset shows a more complex pattern with significant uncertainty. Therefore, the forecasting distribution  $p(y|x)$  in this task should be much simpler than the wind power bidding task.

In this particular scenario, DFL demonstrates minimal model mismatch error and sample average approximation error, given that  $p(y|x)$  is a simple distribution and exhibits low uncertainty. It is worth noting that even with a large number of components in the Gaussian Mixture Model (GMM), the location of each mode should still be very close to each other for this simple distribution, resulting in small errors. Moreover, DFL does not suffer from the gradient approximation error for the convex objective. Consequently, in this task, DFL has the potential to outperform  $DF^2$ .

## 7.2 Additional Ablation Studies

In this subsection, we conduct some additional ablation studies on the wind power bidding task to analyze  $DF^2$ .

**Additional ablation study 1:** The number of samples used to estimate the expected objective in DFL is an important hyperparameter. To investigate its impact, we compare the decision regret and training time of  $DF^2$  with DFL using different numbers of samples. We GMM with 1000 components in the DFL forecaster as it achieves the best performance shown in Section 5.2. As shown in Fig. 10, when the number of samples for DFL exceeds 100, the performance improvement becomes very marginal (64.52 with 100 samples vs. 64.07 with 200 samples). However, the training time increases significantly (1878 seconds/epoch with 100 samples vs. 5251 seconds/epoch with 200 samples). In contrast,  $DF^2$  achieves significantly better decision regret (58.41) while being orders of magnitude faster (2.17 seconds/epoch).

**Additional ablation study 2:** In  $DF^2$ , the value embeddings are initialized with randomly sampled labels from the training set and then updated during the training process. An alternative is to directly use these randomly selected labels and keep the value embeddings fixed during the training process. We examine whether making the value embeddings learnable improves the performance. The results are shown in Fig. 11(a). As we can see, with learnable value embeddings, the decision regret of  $DF^2$  drops significantly compared with the fixed value embeddings.

**Additional ablation study 3:** In  $DF^2$ , we need to sample actions for each  $(x, y)$  pair at each training iteration to fit the function. In this study, we investigate the influence of the number of action samples on the performance. As shown in Fig. 11(b), the decision regret remains stable even for a sample size of 5. Notably, as the number of action samples increases, the variance of the decision regret across different random seeds decreases, indicating improved stability in the results.

## 7.3 Additional Background on Conditional Mean Embedding

We provide more details about how to compute conditional mean embedding (CME) in this subsection.



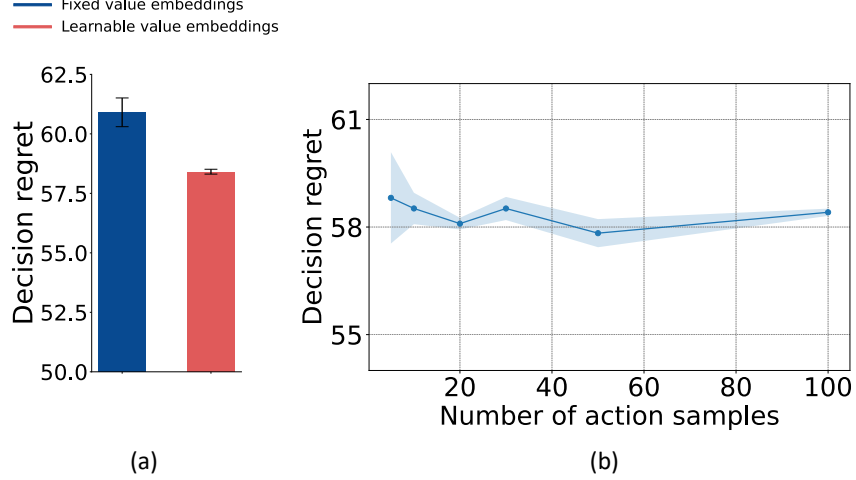


Figure 11: Additional ablation study 2 and 3 on the wind power bidding task.

Let  $\mathcal{F}$  be a reproducing kernel Hilbert space (RKHS) over the domain of  $\mathbf{y}$  with kernel function  $\mathcal{R}_y(\mathbf{y}, \mathbf{y}')$  and inner product  $\langle \cdot, \cdot \rangle_{\mathcal{F}}$ . Its inner product  $\langle \cdot, \cdot \rangle_{\mathcal{F}}$  satisfies the reproducing property:

$$\langle f(\cdot), \mathcal{R}_y(\mathbf{y}, \cdot) \rangle_{\mathcal{F}} = f(\mathbf{y}),$$

meaning that we can view the evaluation of a function  $f \in \mathcal{F}$  at any point  $\mathbf{y}$  as an inner product and the linear evaluation operator is given by  $\mathcal{R}_y(\mathbf{y}, \cdot)$ , *i.e.*, the kernel function. Alternatively,  $\mathcal{R}(\mathbf{y}, \cdot)$  can also be viewed as a feature map  $\varphi(\mathbf{y})$  where  $\mathcal{R}_y(\mathbf{y}, \mathbf{y}') = \langle \varphi(\mathbf{y}), \varphi(\mathbf{y}') \rangle_{\mathcal{F}}$ . Similarly, we can define the RKHS  $\mathcal{G}$  over the domain of  $\mathbf{x}$  with kernel function  $\mathcal{R}_x(\mathbf{x}, \mathbf{x}')$ .

For a particular  $\mathbf{a}$ , we denote the corresponding function with respect to  $\mathbf{y}$  as  $f_{\mathbf{a}}(\mathbf{y})$ . CME projects the conditional distribution to its expected feature map  $\mu_{\mathbf{y}|\mathbf{x}} \triangleq \mathbb{E}_{p(\mathbf{y}|\mathbf{x})}[\mathcal{R}_y(\mathbf{y}, \cdot)]$  and evaluates the conditional expectation of any RKHS function,  $f_{\mathbf{a}} \in \mathcal{F}$ , as an inner product in  $\mathcal{F}$  using the reproducing property:

$$\mathbb{E}_{p(\mathbf{y}|\mathbf{x})}[f_{\mathbf{a}}] = \int p(\mathbf{y}|\mathbf{x}) \langle \mathcal{R}_y(\mathbf{y}, \cdot), f_{\mathbf{a}} \rangle_{\mathcal{F}} d\mathbf{y} = \left\langle \int p(\mathbf{y}|\mathbf{x}) \mathcal{R}_y(\mathbf{y}, \cdot) d\mathbf{y}, f_{\mathbf{a}} \right\rangle_{\mathcal{F}} = \langle \mu_{\mathbf{y}|\mathbf{x}}, f_{\mathbf{a}} \rangle_{\mathcal{F}}. \quad (7)$$

Assume that for all  $f_{\mathbf{a}} \in \mathcal{F}$ , the conditional expectation  $\mathbb{E}_{p(\mathbf{y}|\mathbf{x})}[f_{\mathbf{a}}(\mathbf{y})]$  is an element of  $\mathcal{G}$ , the conditional embedding can be estimated with a finite dataset  $\{\mathbf{x}_s, \mathbf{y}_s\}_{s=1}^S$  as [45, 43]:

$$\hat{\mu}_{\mathbf{y}|\mathbf{x}} = \Phi(\mathbf{K} + \lambda \mathbf{I})^{-1} \mathcal{R}_x(\mathbf{X}, \mathbf{x}) = \sum_{s=1}^S \beta_s(\mathbf{x}) \mathcal{R}_y(\mathbf{y}_s, \cdot), \quad (8)$$

where  $\Phi = (\mathcal{R}_y(\mathbf{y}_1, \cdot), \dots, \mathcal{R}_y(\mathbf{y}_S, \cdot))$  is the feature matrix;  $\mathbf{K} = \Upsilon^{\top} \Upsilon$  is the Gram matrix for samples from variable  $\mathbf{x}$  with  $\Upsilon = (\mathcal{R}_x(\mathbf{x}_1, \cdot), \dots, \mathcal{R}_x(\mathbf{x}_S, \cdot))$ ;  $\mathcal{R}_x(\mathbf{X}, \mathbf{x}) = (\mathcal{R}_x(\mathbf{x}_1, \mathbf{x}), \dots, \mathcal{R}_x(\mathbf{x}_S, \mathbf{x}))^{\top}$ ;  $\lambda$  is the additional regularization parameter to avoid overfitting. Though the assumption  $\mathbb{E}_{p(\mathbf{y}|\mathbf{x})}[f_{\mathbf{a}}(\mathbf{y})] \in \mathcal{G}$  is not necessarily true for continuous domains, existing works treat the expression as an approximation [45] and works well in practice.

One advantage of CME is that  $\hat{\mu}_{\mathbf{y}|\mathbf{x}}$  can converge to  $\mu_{\mathbf{y}|\mathbf{x}}$  in the RKHS norm at an overall rate of  $\mathcal{O}(S^{-\frac{1}{2}})$  [45], which is independent of the input dimensions. This property let CME works well in the high-dimensional space.

As we can see from Eq. 8, the empirical estimator of CME,  $\hat{\mu}_{\mathbf{y}|\mathbf{x}}$ , applies non-uniform weights,  $\beta_s$ , on observations which are, in turn, determined by the conditioning variable  $\mathbf{x}$ .

#### 7.4 Proof of Proposition 1

*Proof.* The training set consists of the given  $\mathcal{D} = \{\mathbf{x}_i, \mathbf{y}_i\}_{i=1}^N$  augmented with the sampled actions  $\mathbf{a}$ . We denote the augmented dataset as  $\mathcal{D}'$ . We assume the fitted function is in a hypothesis  $g^*(\mathbf{x}, \mathbf{a})$ .

Let  $g_{\mathcal{D}'}^*(\mathbf{x}, \mathbf{a})$  denote the function fitted on the dataset  $\mathcal{D}'$ . The expectation of the mean squared error (MSE) for a given unseen test sample, over all possible learning sets, is:

$$\begin{aligned}
& \mathbb{E}_{\mathcal{D}'} [(\mathbb{E}_{p(\mathbf{y}|\mathbf{x})}[f(\mathbf{y}, \mathbf{a})] - g_{\mathcal{D}'}^*(\mathbf{x}, \mathbf{a}))^2] \\
&= \mathbb{E}_{\mathcal{D}'} \left[ \left( \underbrace{\mathbb{E}_{p(\mathbf{y}|\mathbf{x}^*)}[f(\mathbf{y}, \mathbf{a})] - \mathbb{E}_{\mathcal{D}'}[g_{\mathcal{D}'}^*(\mathbf{x}, \mathbf{a})]}_a + \underbrace{\mathbb{E}_{\mathcal{D}'}[g_{\mathcal{D}'}^*(\mathbf{x}, \mathbf{a})] - g_{\mathcal{D}'}^*(\mathbf{x}, \mathbf{a})}_b \right)^2 \right] \\
&= \mathbb{E}_{\mathcal{D}'} [(a + b)^2] \\
&= \mathbb{E}_{\mathcal{D}'} [a^2] + \mathbb{E}_{\mathcal{D}'} [b^2] + \mathbb{E}_{\mathcal{D}'} [2ab]
\end{aligned}$$

The first two terms represent the bias and variance errors respectively:

$$\mathbb{E}_{\mathcal{D}'} [a^2] = \mathbb{E}_{\mathcal{D}'} \left[ (g_{\mathcal{D}'}^*(\mathbf{x}, \mathbf{a}) - \mathbb{E}_{p(\mathbf{y}|\mathbf{x})}[f(\mathbf{y}, \mathbf{a})])^2 \right] = \text{Bias}^2(g^*).$$

$$\mathbb{E}_{\mathcal{D}'} [b^2] = \mathbb{E}_{\mathcal{D}'} \left[ (g_{\mathcal{D}'}^*(\mathbf{x}, \mathbf{a}) - \mathbb{E}_{\mathcal{D}'}[g_{\mathcal{D}'}^*(\mathbf{x}, \mathbf{a})])^2 \right] = \text{Variance}(g^*),$$

Next, we prove the cross-term  $\mathbb{E}_{\mathcal{D}'} [2ab] = 0$ . To simplify the notation, let  $\bar{g}$  denote  $\mathbb{E}_{\mathcal{D}'} [g_{\mathcal{D}'}^*(\mathbf{x}, \mathbf{a})]$ ;  $g$  denote  $g_{\mathcal{D}'}^*(\mathbf{x}, \mathbf{a})$ ;  $\tilde{f}$  denote  $\mathbb{E}_{p(\mathbf{y}|\mathbf{x})}[f(\mathbf{y}, \mathbf{a})]$ . Then we can obtain:

$$\begin{aligned}
& \mathbb{E}_{\mathcal{D}'} \left[ 2(g - \bar{g})(\bar{g} - \tilde{f}) \right] \\
&= 2 \cdot \mathbb{E}_{\mathcal{D}'} [g \cdot \bar{g} - g \cdot \tilde{f} - \bar{g} \cdot \bar{g} + \bar{g} \cdot \tilde{f}] \\
&= 2 \cdot \mathbb{E}_{\mathcal{D}'} [g] \cdot \bar{g} - 2 \cdot \mathbb{E}_{\mathcal{D}'} [g] \cdot \tilde{f} - 2 \cdot \mathbb{E}_{\mathcal{D}'} [\bar{g}^2] + 2 \cdot \tilde{f} \cdot \mathbb{E}_{\mathcal{D}'} [\bar{g}] \\
&= 2 \cdot \bar{g}^2 - 2 \cdot \bar{g} \cdot \tilde{f} - 2 \cdot \bar{g}^2 + 2 \cdot \tilde{f} \cdot \bar{g} \\
&= 0
\end{aligned}$$

Hence, the expectation of the MSE for a given test sample  $\mathbf{x}^*$  is expressed as:

$$\begin{aligned}
\text{MSE}_{\text{test}} &= \mathbb{E}_{\mathcal{D}'} [(\mathbb{E}_{p(\mathbf{y}|\mathbf{x})}[f(\mathbf{y}, \mathbf{a})] - g_{\mathcal{D}'}^*(\mathbf{x}, \mathbf{a}))^2] \\
&= \underbrace{\mathbb{E}_{\mathcal{D}'} \left[ (g_{\mathcal{D}'}^*(\mathbf{x}, \mathbf{a}) - \mathbb{E}_{p(\mathbf{y}|\mathbf{x})}[f(\mathbf{y}, \mathbf{a})])^2 \right]}_{\text{Bias}} + \underbrace{\mathbb{E}_{\mathcal{D}'} \left[ (g_{\mathcal{D}'}^*(\mathbf{x}, \mathbf{a}) - \mathbb{E}_{\mathcal{D}'}[g_{\mathcal{D}'}^*(\mathbf{x}, \mathbf{a})])^2 \right]}_{\text{Variance}} \quad (9)
\end{aligned}$$

Since the training dataset consists of  $\mathbf{x}, \mathbf{y}, \mathbf{a}$ , and each  $\mathbf{y}$  corresponds to a specific  $\mathbf{x}$  from  $\mathcal{D}$ , we can replace the expectation  $\mathbb{E}_{\mathcal{D}'}[\cdot]$  in Eq. 9 with  $\mathbb{E}_{\mathbf{x}, \mathbf{a}}[\cdot]$  and recover Proposition 1.  $\square$

## 7.5 Proof of Proposition 2

*Proof.* We first define the conditional kernel density estimator (KDE),  $\hat{p}_{\mathcal{R}}(\mathbf{y}|\mathbf{x})$ , as follows,

$$\hat{p}_{\mathcal{R}}(\mathbf{y}|\mathbf{x}) = \frac{\sum_{s=1}^S \mathcal{R}_x(\mathbf{k}_s, \mathbf{q}(\mathbf{x})) \mathcal{R}_y(\mathbf{y}_s, \mathbf{y})}{\sum_{s=1}^S \mathcal{R}_x(\mathbf{k}_s, \mathbf{q}(\mathbf{x}))}, \quad (10)$$

Then, we can obtain

$$\begin{aligned}
\mathbb{E}_{\hat{p}_{\mathcal{R}}(\mathbf{y}|\mathbf{x})}[f(\mathbf{y}, \mathbf{a})] &= \int \frac{\sum_{s=1}^S \mathcal{R}_x(\mathbf{k}_s, \mathbf{q}(\mathbf{x})) \mathcal{R}_y(\mathbf{y}_s, \mathbf{y})}{\sum_{s=1}^S \mathcal{R}_x(\mathbf{k}_s, \mathbf{q}(\mathbf{x}))} f(\mathbf{y}, \mathbf{a}) d\mathbf{y} \\
&= \frac{\sum_{s=1}^S \mathcal{R}_x(\mathbf{k}_s, \mathbf{q}) \int \mathcal{R}_y(\mathbf{y}_s, \mathbf{y}) f(\mathbf{y}, \mathbf{a}) d\mathbf{y}}{\sum_{s=1}^S \mathcal{R}_x(\mathbf{k}_s, \mathbf{q}(\mathbf{x}))} \\
&= \frac{\sum_{s=1}^S \mathcal{R}_x(\mathbf{k}_s, \mathbf{q}(\mathbf{x})) (f(\mathbf{y}_s, \mathbf{a}) + \epsilon)}{\sum_{s=1}^S \mathcal{R}_x(\mathbf{k}_s, \mathbf{q}(\mathbf{x}))} \quad (11)
\end{aligned}$$

We next prove that the  $L_1$  norm of the residue term goes to zero, *i.e.*,  $\|\epsilon\|_1 \rightarrow 0$ , under the condition that  $\hat{p}_{\mathcal{R}}(\mathbf{y}|\mathbf{x}) \rightarrow p(\mathbf{y}|\mathbf{x})$  uniformly as  $S \rightarrow \infty$ . To prove this, we follow [9] and assume that  $\mathcal{R}_y(\mathbf{y}, \mathbf{y}') = \mathcal{R}_y(\mathbf{y} - \mathbf{y}')$  is a  $(\eta; \nu)$  valid kernel [9] which satisfies the following property:

$\int \mathbf{z}^{\mathbf{a}} \mathcal{R}_y(\mathbf{y}) d\mathbf{y} = 0$ , for any  $\mathbf{a} = (a_1, \dots, a_d) \in \mathbb{N}^d$  such that  $1 \leq |\mathbf{a}| \leq \lfloor \eta \rfloor$ . In addition,  $\int \|\mathbf{y}\|^\eta |\mathcal{R}_y(\mathbf{y})| d\mathbf{y} \leq \nu$  for some  $\nu > 0$ .

Notice that all spherically symmetric compactly supported probability densities and product kernels based on compactly supported symmetric univariate densities satisfy the properties. For instance, the kernel  $\mathcal{R}(\mathbf{y}) = (2\pi)^{-d/2} \exp(-\|\mathbf{y}\|^2/2)$  satisfies the conditions with  $\beta = \infty$ . We denote  $\mathcal{R}_y^h(\mathbf{y}) = \frac{1}{h^d} \mathcal{R}_y(\frac{\mathbf{y}}{h})$  as the kernel with bandwidth  $h$ .

For a particular  $\mathbf{a}$ , we denote the corresponding function with respect to  $\mathbf{y}$  as  $f_{\mathbf{a}}(\mathbf{y})$ . Also following [9], we assume that  $f_{\mathbf{a}}(\mathbf{y})$  is a Hölder function which satisfies:

(i) for any  $\mathbf{y}_0$ , there exists  $L(\mathbf{y}_0) > 0$  such that

$$|f(\mathbf{y}) - f_{\mathbf{a}}^{(\eta; \mathbf{y}_0)}(\mathbf{y})| \leq L(\mathbf{y}_0) \|\mathbf{y} - \mathbf{y}_0\|^\eta, \forall \mathbf{y} \in \mathcal{Y},$$

where  $f_{\mathbf{a}}^{(\eta; \mathbf{y}_0)}$  is the  $\lfloor \eta \rfloor$ -order Taylor approximation at  $\mathbf{y}_0$ .

(ii) in addition, the integral  $\int L(\mathbf{y}) d\mathbf{y} \leq \mathcal{L}$ .

**Lemma 1.** *If  $\mathcal{R}_y$  is a  $(\eta; \nu)$  valid kernel and  $f_{\mathbf{a}}(\mathbf{y})$  is a Hölder function, then*

$$\|\epsilon\|_1 = \left\| \int \mathcal{R}_y^h(\mathbf{y}_s, \mathbf{y}) f(\mathbf{y}, \mathbf{a}) d\mathbf{y} - f(\mathbf{y}_s, \mathbf{a}) \right\|_1 \leq \nu \mathcal{L} h^\eta. \quad (12)$$

*Proof.* The proof of this lemma follows directly from Chapter 4.3 in [53].

$$\begin{aligned} |\epsilon| &= \left| \int \mathcal{R}_y^h(\mathbf{y}_s, \mathbf{y}) f_{\mathbf{a}}(\mathbf{y}) d\mathbf{y} - f_{\mathbf{a}}(\mathbf{y}_s) \right| \\ &= \left| \int \frac{1}{h^d} \mathcal{R}_y\left(\frac{\mathbf{y} - \mathbf{y}_s}{h}\right) f_{\mathbf{a}}(\mathbf{y}) d\mathbf{y} - f_{\mathbf{a}}(\mathbf{y}_s) \right| \\ &= \left| \int \frac{1}{h^d} \mathcal{R}_y\left(\frac{\mathbf{y}}{h}\right) [f_{\mathbf{a}}(\mathbf{y}_s + \mathbf{y}) - f_{\mathbf{a}}(\mathbf{y}_s)] d\mathbf{y} \right| \\ &= \left| \int \mathcal{R}_y(\mathbf{y}) [f_{\mathbf{a}}(\mathbf{y}_s + h\mathbf{y}) - f_{\mathbf{a}}(\mathbf{y}_s)] d\mathbf{y} \right| \\ &\leq \left| \int \mathcal{R}_y(\mathbf{y}) [f_{\mathbf{a}}(\mathbf{y}_s + h\mathbf{y}) - f_{\mathbf{a}}^{(\eta; \mathbf{y}_s)}(\mathbf{y}_s + h\mathbf{y})] d\mathbf{y} \right| \\ &\quad + \left| \int \mathcal{R}_y(\mathbf{y}) [f_{\mathbf{a}}^{(\eta; \mathbf{y}_s)}(\mathbf{y}_s + h\mathbf{y}) - f_{\mathbf{a}}(\mathbf{y}_s)] d\mathbf{y} \right| \\ &\leq L(\mathbf{y}) \int |\mathcal{R}_y(\mathbf{y})| \|h\mathbf{y}\|^\eta d\mathbf{y} + \left| \int \mathcal{R}_y(\mathbf{y}) [f_{\mathbf{a}}^{(\eta; \mathbf{y}_s)}(\mathbf{y}_s + h\mathbf{y}) - f_{\mathbf{a}}(\mathbf{y})] d\mathbf{y} \right| \end{aligned}$$

Note that  $f_{\mathbf{a}}^{(\eta; \mathbf{y}_s)}(\mathbf{y}_s + h\mathbf{y}) - f_{\mathbf{a}}(\mathbf{y})$  is a polynomial of degree at most  $\lfloor \eta \rfloor$  with no constant, by the definition of  $(\eta; \nu)$ -valid density kernel, the second term is zero. Hence, we have  $|\epsilon| \leq \nu L(\mathbf{y}) h^\eta$ , and therefore

$$\|\epsilon\|_1 \leq \nu h^\eta \int L(\mathbf{y}) d\mathbf{y} \leq \nu \mathcal{L} h^\eta. \quad \square$$

As we can see from Lemma 1, the  $L_1$  norm of the residue term is bounded by  $\nu \mathcal{L} h^\eta$ . According to [14], when  $\hat{p}_{\mathcal{R}}(\mathbf{y}|\mathbf{x}) \rightarrow p(\mathbf{y}|\mathbf{x})$  uniformly as  $S \rightarrow \infty$ , the bandwidth of the kernel should go to zero, *i.e.*,  $h \rightarrow 0$ . Hence we obtain  $\|\epsilon\|_1 \rightarrow 0$ , which further leads to:

$$\mathbb{E}_{\hat{p}_{\mathcal{R}}(\mathbf{y}|\mathbf{x})}[f(\mathbf{y}, \mathbf{a})] \rightarrow \frac{\sum_{s=1}^S \mathcal{R}_x(\mathbf{k}_s, \mathbf{q}(\mathbf{x})) f(\mathbf{y}_s, \mathbf{a})}{\sum_{s=1}^S \mathcal{R}_x(\mathbf{k}_s, \mathbf{q}(\mathbf{x}))}.$$

When  $\mathcal{R}_x(\mathbf{k}, \mathbf{q})$  is an exponential kernel. *i.e.*,  $\mathcal{R}_x(\mathbf{k}, \mathbf{q}) = \exp\left(\frac{\mathbf{q}^\top \mathbf{k}}{\sqrt{d}}\right)$ , we can obtain

$$\begin{aligned} \mathbb{E}_{\hat{p}_{\mathcal{R}}(\mathbf{y}|\mathbf{x})}[f(\mathbf{y}, \mathbf{a})] &= \frac{\sum_{s=1}^S \mathcal{R}_x(\mathbf{k}_s, \mathbf{q}(\mathbf{x})) f(\mathbf{y}_s, \mathbf{a})}{\sum_{s=1}^S \mathcal{R}_x(\mathbf{k}_s, \mathbf{q}(\mathbf{x}))} \\ &= \frac{\sum_{s=1}^S \exp\left(\frac{\mathbf{q}(\mathbf{x})^\top \mathbf{k}_s}{\sqrt{d}}\right) f(\mathbf{y}_s, \mathbf{a})}{\sum_{s=1}^S \exp\left(\frac{\mathbf{q}(\mathbf{x})^\top \mathbf{k}_s}{\sqrt{d}}\right)} \\ &= \text{Softmax}\left(\left[\frac{\mathbf{q}(\mathbf{x})^\top \mathbf{k}_1}{\sqrt{d}}, \dots, \frac{\mathbf{q}(\mathbf{x})^\top \mathbf{k}_S}{\sqrt{d}}\right]\right)^\top [f(\mathbf{v}_1, \mathbf{a}), \dots, f(\mathbf{v}_S, \mathbf{a})] \\ &= g(\mathbf{x}, \mathbf{a}). \end{aligned} \quad (13)$$

The second last equation comes from the definition of the softmax function and replacing the notation  $\mathbf{y}$  with  $\mathbf{v}$  which is commonly used in the existing literature.

Therefore, under the condition that  $\hat{p}_{\mathcal{R}}(\mathbf{y}|\mathbf{x}) \rightarrow p(\mathbf{y}|\mathbf{x})$  uniformly for any  $\mathbf{x}$  as  $S \rightarrow \infty$ , we have:

$$g(\mathbf{x}, \mathbf{a}) = \mathbb{E}_{\hat{p}_{\mathcal{R}}(\mathbf{y}|\mathbf{x})}[f(\mathbf{y}, \mathbf{a})] \rightarrow \mathbb{E}_{p(\mathbf{y}|\mathbf{x})}[f(\mathbf{y}, \mathbf{a})] \quad \text{as } S \rightarrow \infty. \quad (14)$$

Besides the Softmax attention, an alternative attention mechanism is called conditional mean embedding (CME) attention [59] which directly mimics the computation of CME weights  $\beta_s$  in Eq. 8:

$$[\beta_1(\mathbf{x}), \dots, \beta_S(\mathbf{x})] = (\mathcal{R}_x(\mathbf{K}, \mathbf{K}) + \lambda \mathbf{I})^{-1} \mathcal{R}_x(\mathbf{K}, \mathbf{q}(\mathbf{x})), \quad (15)$$

where  $\mathcal{R}_x(\mathbf{K}, \mathbf{q}(\mathbf{x})) \in \mathbb{R}^S$  with  $\mathcal{R}_x(\mathbf{K}, \mathbf{q}(\mathbf{x}))[s] = \mathcal{R}_x(\mathbf{k}_s, \mathbf{q}(\mathbf{x}))$  and  $\mathcal{R}_x(\mathbf{K}, \mathbf{K}) \in \mathbb{R}^{S \times S}$  with  $\mathcal{R}_x(\mathbf{K}, \mathbf{K})[s_1, s_2] = \mathcal{R}_x(\mathbf{k}_{s_1}, \mathbf{k}_{s_2})$ .

With the CME attention, we obtain the corresponding function  $g_{\text{CME}}(\mathbf{x}, \mathbf{a})$ :

$$g_{\text{CME}}(\mathbf{x}, \mathbf{a}) = ((\mathcal{R}_x(\mathbf{K}, \mathbf{K}) + \lambda \mathbf{I})^{-1} \mathcal{R}_x(\mathbf{K}, \mathbf{q}(\mathbf{x})))^\top [f(\mathbf{v}_1, \mathbf{a}), \dots, f(\mathbf{v}_S, \mathbf{a})]. \quad (16)$$

According to [59], CME attention converges to the kernel conditional mean embedding. It holds with probability at least  $1 - \delta$  that

$$\|g_{\text{CME}}(\mathbf{x}, \mathbf{a}) - \mathbb{E}_{p(\mathbf{y}|\mathbf{x})}[f(\mathbf{y}, \mathbf{a})]\|_2 = \mathcal{O}\left(\sqrt{\frac{S}{\lambda}} \cdot \left(\frac{2}{\lambda} + \sqrt{\frac{\Gamma(S^{-1})\lambda}{\lambda}}\right) \log \frac{1}{\delta} + \lambda S^{-1}\right), \quad (17)$$

where  $\Gamma(S^{-1}\lambda)$  is the effective dimension of the covariance operator.

Note that the CME attention is essentially a variant of the Softmax attention [50] with a different normalization. In our work, we choose to use the Softmax attention which has achieved success in many deep learning applications. *Existing work[59] has also shown that Softmax attention has the same limit as CME attention as  $S \rightarrow \infty$ .*

□

## 7.6 Experimental Details

### 7.6.1 Synthetic Data

**Data generation process:** We generate the synthetic dataset following a mixture of three Gaussians:

$$\mathbf{x} \sim \mathcal{U}^2[-1, 1], \quad \mathbf{y} \sim 0.3\mathcal{N}(\mathbf{A}_1\mathbf{x}, 0.1 \cdot \mathbf{I}) + 0.3\mathcal{N}(\mathbf{A}_2\mathbf{x}, 0.1 \cdot \mathbf{I}) + 0.4\mathcal{N}(\mathbf{A}_3\mathbf{x}, 0.1 \cdot \mathbf{I}), \quad (18)$$

where the elements of  $\mathbf{A}_1, \mathbf{A}_2, \mathbf{A}_3 \in \mathbb{R}^{2 \times 2}$  are uniformly sampled from  $\mathcal{U}[0, 1]$ .

We generate 5000  $(\mathbf{x}, \mathbf{y})$  pairs, randomly dividing them into a training set (70%, 3500 pairs), and equal validation and testing sets (15% each, 750 pairs).

**Optimization objective:** We consider both the convex and non-convex objectives.

Convex objective:

$$\text{minimize}_{\mathbf{a} \in \mathbb{R}^2} \mathbb{E}_{p(\mathbf{y}|\mathbf{x})} \sum_{i=1}^2 [5(\mathbf{y}[i] - \mathbf{a}[i])_+ + 20(\mathbf{a}[i] - \mathbf{y}[i])_+ + 0.5(\mathbf{y}[i] - \mathbf{a}[i])_+^2 + 0.2(\mathbf{a}[i] - \mathbf{y}[i])_+^2]$$

subject to  $-1 \leq \mathbf{a}[i] \leq 1, \forall i$ .

Non-convex objective:

$$\begin{aligned} & \text{minimize}_{\mathbf{a} \in \mathbb{R}^2} \mathbb{E}_{p(\mathbf{y}|\mathbf{x})} \sum_{i=1}^2 [10(\mathbf{y}[i] - \mathbf{a}[i])_+^2 + 2(\mathbf{a}[i] - \mathbf{y}[i])_+^2 + 4\mathbf{a}[i]^3] \\ & \text{subject to} \quad -2 \leq \mathbf{a}[i] \leq 2, \forall i, \end{aligned}$$

where  $(v)_+$  denote  $\max\{v, 0\}$ .

**Solver at test time:** At test time, for a fair comparison, we use the same optimization solver for all the methods. Specifically, we use projected gradient descent and the gradient update step adopts the Adam [25] optimizer. The learning rate is 0.01 and we repeat 500 iterations. We empirically found that this solver solves this optimization problem very well.

**Model Hyperparameters:** For the two-stage model, DFL and SO-EBM, the forecaster uses GMM with a different number of components and use 100 samples to estimate the expectation of the objective as we found that more samples bring little performance gain. The forecaster uses a neural network with one hidden layer as the feature extractor which is further stacked by a linear layer. This network has a hidden size of 128, employing ReLU as the nonlinear activation function. The forecaster outputs the mean, log variance, and weight for each GMM component. During training, we sample from the GMM using the Gumbel softmax trick [18] to make the sampling process differentiable. SO-EBM draws 512 samples from the proposal distribution to estimate the gradient of the model parameters. The proposal distribution is a mixture of Gaussians with 3 components where the variances are  $\{0.01, 0.02, 0.05\}$ .

For a fair comparison, DF<sup>2</sup> uses the same feature extractor for the encoder. The attention architecture uses 1000 attention points for both the convex and non-convex objectives. During training, DF<sup>2</sup> samples 100 actions  $\mathbf{a}$  uniformly from the constrained space, *i.e.*, the box, for each  $(\mathbf{x}, \mathbf{y})$  pair at each iteration for function fitting.

**Model Optimization:** We use the Adam [25] algorithm for model optimization. The number of training epochs is 50. The learning rate for all the methods is  $10^{-3}$ . DFL and SO-EBM use the two-stage model as the pre-trained model for faster training convergence.

## 7.6.2 Wind Power Bidding

**Optimization objective:** In this task, a wind power firm engages in both energy and reserve markets, given the generated wind power  $\mathbf{x} \in \mathbb{R}^{24}$  in the last 24 hours. The firm needs to decide the energy quantity  $\mathbf{a}_E \in \mathbb{R}^{12}$  to bid and quantity  $\mathbf{a}_R \in \mathbb{R}^{12}$  to reserve over the upcoming 12th-24th hours in advance, based on the forecasted wind power  $\mathbf{y} \in \mathbb{R}^{12}$ . The optimization objective is to maximize the profit which is a piecewise function consisting of three segments [6, 39]:

$$\begin{aligned} & \text{maximize}_{\mathbf{a}_E \in \mathbb{R}^{12}, \mathbf{a}_R \in \mathbb{R}^{12}} \mathbb{E}_{p(\mathbf{y}|\mathbf{x})} \sum_{i=1}^{12} P\mathbf{y}[i] - \nu\mathbf{a}_R[i] \\ & + \begin{cases} -\Delta P_{\text{up},1}(\mathbf{a}_E[i] - \mathbf{a}_R[i] - \mathbf{y}[i]) - \Delta P_{\text{up},2}(\mathbf{a}_E[i] - \mathbf{a}_R[i] - \mathbf{y}[i])^2 - \mu\mathbf{a}_R[i] - F, & \text{if } \mathbf{y}[i] < \mathbf{a}_E[i] - \mathbf{a}_R[i] \\ -\mu(\mathbf{a}_E[i] - \mathbf{y}[i]), & \text{if } \mathbf{a}_E[i] - \mathbf{a}_R[i] \leq \mathbf{y}[i] \leq \mathbf{a}_E[i] \\ -\Delta P_{\text{down}}(\mathbf{y}[i] - \mathbf{a}_E[i]), & \text{if } \mathbf{y}[i] > \mathbf{a}_E[i] \end{cases} \\ & \text{subject to} \quad E_{\min} \leq \mathbf{a}_E[i] \leq E_{\max}, R_{\min} \leq \mathbf{a}_R[i] \leq R_{\max}, \quad \forall i. \end{aligned}$$

$P$  is the regular price of the wind energy sold,  $\mathbf{y}[i]$  is the energy generated during period  $i$ ,  $\mathbf{a}_E[i]$  and  $\mathbf{a}_R[i]$  are the bid and up reserve energy volumes for period  $i$ , respectively.  $\nu$  corresponds to the opportunity cost when the company participates in the reserve markets, and  $\mu$  is the deploy price of the reserved energy. This structure encapsulates three market participation scenarios. In the scenario where  $\mathbf{y}[i] < \mathbf{a}_E[i] - \mathbf{a}_R[i]$ , the company overbids, consequently deploying all reserved energy and facing a linear overbidding penalty, a quadratic overbidding penalty and a constant penalty determined by coefficients  $\Delta P_{\text{up},1}$ ,  $\Delta P_{\text{up},2}$ , and  $F$ . If  $\mathbf{a}_E[i] - \mathbf{a}_R[i] \leq \mathbf{y}[i] \leq \mathbf{a}_E[i]$ , the company meets its bid by deploying reserve market energy, thereby avoiding penalties. In this case, the company only needs to pay the deployment fee for the reserved energy. However, when  $\mathbf{y}[i] > \mathbf{a}_E[i]$ , the company underbids, resulting in the selling of surplus electricity at a discount and incurring losses defined by the coefficient  $\Delta P_{\text{down}}$ . We set  $P$  as 100, according to the average bidding price obtained from Nord Pool, a European power exchange.  $\nu$  and  $\mu$  are 20 and 110 respectively, as a general setting [6, 39].

The value of  $\Delta P_{\text{up},1}$ ,  $\Delta P_{\text{up},2}$ ,  $\Delta P_{\text{down}}$  and  $F$  are set to 200, 100, 20 and 10, to ensure an effective penalty.  $E_{\text{min}} = 0$ ,  $R_{\text{min}} = 0.15$ , and  $E_{\text{max}} = R_{\text{max}} = 4$ .

According to the optimality condition, the optimal  $\mathbf{a}_R[i]$  is always equal to  $R_{\text{min}}$  for all  $i$ . Therefore, we only need to determine the decision variable  $\mathbf{a}_E$ .

We use the wind power generation dataset of the German energy company TenneT during 08/23/2019 to 09/22/2020<sup>2</sup>. The split ratio of the training dataset, validation dataset, and test dataset are 64%, 16%, 20%, respectively.

**Solver at test time:** At test time, for a fair comparison, we use the same optimization solver for all the methods. Specifically, we use projected gradient descent and the gradient update step adopts the Adam [25] optimizer. The learning rate is 0.1 and we repeat 500 iterations. We empirically found that this solver solves this optimization problem very well.

**Model Hyperparameters:** For the two-stage model, DFL and SO-EBM, the forecaster uses GMM with a different number of components and use 100 samples to estimate the expectation of the objective as we found that more samples bring little performance gain. The forecaster uses a two-layer long short-term memory network (LSTM) [16] as the feature extractor which is further stacked by a linear layer. The network has a hidden size of 256. It takes the historical wind power in the last 24 hours as input features and outputs the forecasted wind power for the 12th to 24th hours in the future. The forecaster outputs the mean, log variance, and weight for each GMM component. During training, we sample from the GMM using the Gumbel softmax trick [18] to make the sampling process differentiable. SO-EBM draws 512 samples from the proposal distribution to estimate the gradient of the model parameters. The proposal distribution is a mixture of Gaussians with 3 components where the variances are  $\{0.02, 0.05, 0.1\}$ .

For a fair comparison, DF<sup>2</sup> uses the same LSTM architecture as the encoder and 500 attention points. During training, we sample 100 actions  $\mathbf{a}$  uniformly from the constrained space for each  $(\mathbf{x}, \mathbf{y})$  pair at each iteration.

**Model Optimization:** We use the Adam [25] algorithm for model optimization. The number of training epochs is 200. The learning rate for all the methods is  $10^{-3}$ . DFL and SO-EBM use the two-stage model as the pre-trained model for faster training convergence.

### 7.6.3 COVID-19 Vaccine Distribution

**Optimization objective:** In this task, given the OD matrices  $\mathbf{x} \in \mathbb{R}^{47 \times 47 \times 7}$  of last week, *i.e.*,  $\mathbf{x}[i, j, t]$  represents the number of people move from region  $i$  to  $j$  on day  $t$ , we need to decide the vaccine distribution  $\mathbf{a} \in \mathbb{R}^{47}$  across the 47 regions in Japan with a budget constraint ( $\mathbf{a}[i]$  is the number of vaccines distributed to the region  $i$ ). The optimization objective is to minimize the total number of infected people over the ODE-driven dynamics, based on the forecasted OD matrices  $\mathbf{y} \in \mathbb{R}^{47 \times 47 \times 7}$  for the next week.

We want to distribute the vaccine over each county to minimize the number of infected cases. The number of infected cases is given by a metapopulation SEIRV model [30, 35], denoted by Simulator( $\cdot, \cdot$ ):

$$\begin{aligned} & \arg \min_{\mathbf{a} \in \mathbb{R}^{47}} \mathbb{E}_{p(\mathbf{y}|\mathbf{x})} [\text{Simulator}(\mathbf{y}, \mathbf{a})], \\ & \text{Subject to } \sum_i \mathbf{a}[i] \leq \text{Budget}, \mathbf{a}[i] \geq 0. \end{aligned}$$

We use the OD matrices dataset of Japan<sup>3</sup> during 04/01/2020 to 02/28/2021. The split ratio of the training dataset, validation dataset, and test dataset are 64%, 16%, 20%, respectively. We set the budget as  $5 \times 10^6$ .

**Details of the simulator:** The SEIRV model is an epidemiological model used to predict and understand the spread of infectious diseases. It divides the population into five compartments: Susceptible (S), Exposed (E), Infectious (I), Recovered (R) and Vaccined (V). The model is defined by a set of differential equations that describe the transitions between these compartments. There are four hyperparameters in the SEIRV model:

<sup>2</sup>The dataset is available at: <https://www.kaggle.com/datasets/jorgesandoval/wind-power-generation?select=TransnetBW.csv>

<sup>3</sup>The dataset is available at <https://github.com/deepkashiwa20/ODCRN/tree/main/data>

- $\beta$  - Transmission rate: Represents the average number of contacts per person per unit of time multiplied by the probability of disease transmission in a contact between a susceptible and an infectious individual.
- $\sigma$  - Latent rate (or the inverse of the incubation period): The rate at which exposed individuals progress to the infectious state. The incubation period is the time it takes for an individual to become infectious after exposure.
- $\gamma$  - Recovery rate (or the inverse of the infectious period): The rate at which infectious individuals recover or die and transition to the recovered state. The infectious period is the time during which an infected individual can transmit the disease.
- $N$  - Total population: The sum of individuals in all compartments (S, E, I, R, V).

When considering mobility flow among different regions, we need to adapt the SEIRV model to account for the movement of individuals between regions. In this case, the model becomes a spatially explicit, multi-region SEIRV model. Each region will have its own SEIRV model, and the flow of individuals between regions will affect the dynamics of the compartments. Specifically, for each region  $k = 1, \dots, K$ , we have:

$$\begin{aligned}
\frac{d\mathbf{S}[k]}{dt} &= -\beta[k] \frac{\mathbf{S}[k] \cdot \mathbf{I}[k]}{\mathbf{N}[k]} - \frac{\mathbf{S}[k]}{\mathbf{S}[k] + \mathbf{E}[k]} \cdot \frac{\mathbf{a}[k]}{T} + \sum_{i \neq k} \tilde{\mathbf{y}}[i, k, t] \cdot \mathbf{S}[i] - \sum_{j \neq k} \tilde{\mathbf{y}}[k, j, t] \cdot \mathbf{S}[k], \\
\frac{d\mathbf{E}[k]}{dt} &= \beta[k] \frac{\mathbf{S}[k] \cdot \mathbf{I}[k]}{\mathbf{N}[k]} - \sigma[k] \cdot \mathbf{E}[k] - \frac{\mathbf{E}[k]}{\mathbf{S}[k] + \mathbf{E}[k]} \cdot \frac{\mathbf{a}[k]}{T} + \sum_{i \neq k} \tilde{\mathbf{y}}[i, k, t] \cdot \mathbf{E}[i] - \sum_{j \neq k} \tilde{\mathbf{y}}[k, j, t] \cdot \mathbf{E}[k], \\
\frac{d\mathbf{I}[k]}{dt} &= \sigma[k] \cdot \mathbf{E}[k] - \gamma[k] \cdot \mathbf{I}[k] + \sum_{i \neq k} \tilde{\mathbf{y}}[i, k, t] \cdot \mathbf{I}[i] - \sum_{j \neq k} \tilde{\mathbf{y}}[k, j, t] \cdot \mathbf{I}[k], \\
\frac{d\mathbf{R}[k]}{dt} &= \gamma[k] \cdot \mathbf{I}[k] + \sum_{i \neq k} \tilde{\mathbf{y}}[i, k, t] \cdot \mathbf{R}[i] - \sum_{j \neq k} \tilde{\mathbf{y}}[k, j, t] \cdot \mathbf{R}[k], \\
\frac{d\mathbf{V}[k]}{dt} &= \frac{\mathbf{a}[k]}{T} + \sum_{i \neq k} \tilde{\mathbf{y}}[i, k, t] \cdot \mathbf{V}[i] - \sum_{j \neq k} \tilde{\mathbf{y}}[k, j, t] \cdot \mathbf{V}[k], \tag{19}
\end{aligned}$$

where  $\beta[k]$ ,  $\gamma[k]$ , and  $\sigma[k]$  are hyper-parameter for region  $k$ . These hyperparameters are fitted on the dataset using maximum likelihood estimation.  $\tilde{\mathbf{y}}$  is the normalized OD matrix.

Finally, the simulator will output the total number of newly infected people across all the regions and we aim to minimize this value.

**Solver at test time:** At test time, for a fair comparison, we use the same optimization solver for all the methods. Specifically, we use mirror descent [4] so that the updated decision variable will still variable satisfy the constraints. Specifically, the update rule takes the following form at  $t$ -th iteration:

$$\mathbf{a}_{t+1}[i] = \text{Budget} \cdot \frac{\mathbf{a}_t[i] \exp(-\gamma \nabla_i f(\mathbf{a}_t))}{\sum_{j=1}^n \mathbf{a}_t[j] \exp(-\gamma \nabla_j f(\mathbf{a}_t))}, \tag{20}$$

where  $\gamma$  is the learning rate. We set the learning rate as 0.01 and repeat 500 iterations. We empirically found that this solver solves this optimization problem very well.

**Model Hyperparameters:** For the two-stage model, DFL and SO-EBM, the forecaster uses GMM with a different number of components and use 100 samples to estimate the expectation of the objective as we found that more samples bring little performance gain. The forecaster is a DC-RNN [32] which adopts an encoder-decoder architecture. The encoder and decoder both have two hidden layers with a hidden size of 128. The forecaster takes the OD matrices of last week as input features and predicts the OD matrices of next week. The forecaster outputs the mean, log variance, and weight for each GMM component. During training, we sample from the GMM using the Gumbel softmax trick [18] to make the sampling process differentiable. Since the decision variable is a simplex, we train SO-EBM with projected Langevin dynamics. Specifically, at each iteration of the Langevin dynamics, we project the decision variable into the simplex. The number of iterations of the Langevin dynamics is 100 and the step size is 0.05.

For a fair comparison, DF<sup>2</sup> employs the same encoder as the DC-RNN architecture and uses 100 attention points. During training, DF<sup>2</sup> samples 100 actions a uniformly from the constrained space,

*i.e.*, the simplex, for each  $(\mathbf{x}, \mathbf{y})$  pair at each iteration for function fitting. To uniformly sample from the simplex, we sample from the Dirichlet distribution where all parameters are 1.

**Model Optimization:** We use the Adam [25] algorithm for model optimization. The number of training epochs is 50. The learning rate for all the methods is  $10^{-4}$ . DFL and SO-EBM use the two-stage model as the pre-trained model for faster training convergence.

#### 7.6.4 Inventory Optimization

**Solver at test time:** At test time, for a fair comparison, we use the same optimization solver for all the methods. Specifically, we use projected gradient descent and the gradient update step adopts the Adam [25] optimizer. The learning rate is 0.1 and we repeat 500 iterations. We empirically found that this solver solves this optimization problem very well.

**Model Hyperparameters:** The forecaster of the two-stage model, DFL and SO-EBM uses a two-layer long short-term memory network (LSTM) [17] as a feature extractor which is further stacked by a linear layer. The forecaster takes the historical item sales in the last 14 days as input features and outputs the forecasted item sales for the 3rd to 10th days in the future. The network has a hidden size of 128. SO-EBM draws 512 samples from the proposal distribution to estimate the gradient of the model parameters. The proposal distribution is a mixture of Gaussians with 3 components where the variances are  $\{0.05, 0.1, 0.2\}$ .

For a fair comparison, DF<sup>2</sup> uses the same LSTM architecture as the encoder and 230 attention points. During training, the two-stage model, DFL and SO-EBM use 100 samples to estimate the expected objective as more samples provide little performance gain.

**Model Optimization:** We use the Adam [25] algorithm for model optimization. The number of training epochs is 200. The learning rate for all the methods is  $10^{-3}$ . DFL and SO-EBM use the two-stage model as the pre-trained model for faster training convergence.